



January 2014

Retrievals Of The Deep Convective System Ice Cloud Microphysical Properties Using The Arm Radar And Aircraft In-Situ Measurements

Jingjing Tian

Follow this and additional works at: <https://commons.und.edu/theses>

Recommended Citation

Tian, Jingjing, "Retrievals Of The Deep Convective System Ice Cloud Microphysical Properties Using The Arm Radar And Aircraft In-Situ Measurements" (2014). *Theses and Dissertations*. 1722.
<https://commons.und.edu/theses/1722>

This Thesis is brought to you for free and open access by the Theses, Dissertations, and Senior Projects at UND Scholarly Commons. It has been accepted for inclusion in Theses and Dissertations by an authorized administrator of UND Scholarly Commons. For more information, please contact zeinebyousif@library.und.edu.

RETRIEVALS OF THE DEEP CONVECTIVE SYSTEM ICE CLOUD
MICROPHYSICAL PROPERTIES USING THE ARM RADAR AND AIRCRAFT
IN-SITU MEASUREMENTS

by

Jingjing Tian

Bachelor of Science, Nanjing University of Information Science and Technology, 2011

A Thesis

Submitted to the Graduate Faculty

of the

University of North Dakota

In partial fulfillment of the requirements

for the degree of

Master of Science

Grand Forks, North Dakota

August

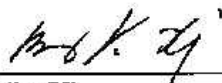
2014

Copyright 2014 Jingjing Tian

This thesis, submitted by Jingjing Tian in partial fulfillment of the requirements for the Degree of Master of Science from the University of North Dakota, has been read by the Faculty Advisory Committee under whom the work has been done and is hereby approved.



Dr. Xiquan Dong




Dr. Baiké Xi

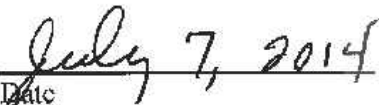


Dr. Mark Anthony Askelson

This thesis is being submitted by the appointed advisory committee as having met all of the requirements of the Graduate School at the University of North Dakota and is hereby approved.



Wayne Swisher
Dean of the Graduate School



Date

PERMISSION

Title Retrievals of the Deep Convective System Ice Cloud Microphysical Properties Using the ARM Radar and Aircraft In-situ Measurements

Department Atmospheric Science

Degree Master of Science

In presenting this thesis in partial fulfillment of the requirements for a graduate degree from the University of North Dakota, I agree that the library of the University shall make it freely available for inspection. I further agree that permission for extensive copying for scholarly purposes may be granted by the professor who supervised my thesis work or, in his absence, by the chairperson of the department or the dean of the Graduate School. It is understood that any copying or publication or other use of the thesis or part thereof for financial gain shall not be allowed without my written permission. It is also understood that due recognition shall be given to me and to the University of North Dakota in any scholarly use which may be made of any material in my thesis.

Jingjing Tian

Date 07-02-2014

TABLE OF CONTENTS

LIST OF FIGURES	vii
LIST OF TABLES	x
ACKNOWLEDGEMENTS.....	xi
ABSTRACT.....	xii
CHAPTER	
I. INTRODUCTION	1
II. DATA AND METHODOLOGY	8
Data.....	8
ARM Ground-based Observations.....	9
Aircraft In-situ Measurements	11
Next Generation Weather Radar (NEXRAD) data.....	17
Discrete Dipole Approximation (DDA) dataset	20
Geostationary Operational Environmental Satellite (GOES) data.....	25
Methodology.....	28
Retrieval Algorithm	28
Sensitivity Studies.....	30
III. RESULTS	36

Radar retrievals	36
Validation with Aircraft In-situ Measurements	39
Validation of the Assumptions in the Radar-based retrieval algorithms	45
Comparisons with GOES Satellite Retrievals.....	47
Cloud-top Height (CTH).....	47
DCS Ice Cloud Particle Size	49
IV. CONCLUSIONS AND FUTURE WORK.....	55
Conclusions	55
Future Work	56
Apply Retrieval Method to NEXRAD	56
Improve Satellite Nighttime Particle Size	59
Development of Algorithms for Retrieving Cloud Microphysical Properties of Mixed-phase and Liquid/precipitation Layers of DCSs during MC3E	60
APPENDIX.....	61
REFERENCES CITED.....	64

LIST OF FIGURES

Figure	Page
1.	(a) Joss-Waldvogel impact disdrometer (JWD)-measured rain rate (red line) and MWR-retrieved cloud LWP (black line), (b) ARM SGP KAZR ARSCL reflectivity (above ground level, AGL) and (c) Combined ARM SGP UAZR calibrated, JWD adjusted KAZR reflectivity.....11
2.	(a) UND Citation II aircraft flight patterns (black lines) over the ARM SGP site during 20 May 2011. (b) ARM SGP corrected KAZR reflectivity with aircraft flight trajectory (thick black line with blue Leg1 and red Leg2) and temperature contours (thin black lines) on 20 May 2011.....13
3.	A series of 2-min averaged particle size distributions (PSDs) derived from a combination of 2DC (30-3,000 μm) and High Volume Precipitation Spectrometer (HVPS, 300 and 30,000 μm) (filled circle) measurements obtained with the UND Citation II Research aircraft on 20 May 2011.....16
4.	(a) The classified DCS components (CC-Convective Core; SR-Stratiform; AC-Anvil Cloud) based on NEXRAD observations using the Feng et al. (2011) CSA classification algorithm with the aircraft flight pattern (black lines) over the ARM SGP site (red diamond) during 14:15-14.32 UTC (Leg 1, SR region of DCS), 20 May 2011. (b) same as (a) except for the period 16:07-16:16 UTC (Leg 2, AC region of DCS).....18
5.	(a) Time series of ARM SGP adjusted KAZR reflectivity during the period 13:00-17:00 UTC when the UND aircraft data are available, (b) NEXRAD cross section at the ARM SGP site and (c) adjusted KAZR reflectivity minus NEXRAD reflectivity.....19
6.	Radar backscatter cross section σ at 35 GHz around -22 $^{\circ}\text{C}$ as a function of maximum dimension D for 11 non-spherical ice crystals (colored lines) calculated using the discrete dipole approximation (DDA) method (Liu, 2008).....22
7.	Comparisons between calculated reflectivity using 4 kinds of bullet rosettes ice habits σ information from DDA database and parameterized bullet rosette σ - D relationship (red lines) for (a) Leg 1 and (b) Leg 2.....22
8.	As in Fig. 6 but for radar backscatter cross section s at 35 GHz from -20 $^{\circ}\text{C}$ to -40 $^{\circ}\text{C}$24

9.	GOES retrieved daytime cloud optical depth τ , cloud top height CTH and particle size D_e at 14:15 UTC on 20 May, 2011.....	27
10.	Dependence of radar-retrieved ice cloud effective radius r_e on N_t and a for a given ice crystal category: (a) bullet rosette, (b) snowflake, (c) plate and (d) column habits.....	31
11.	As in Fig. 10 but for retrieved cloud IWC	32
12.	Dependence of radar-retrieved ice cloud r_e and IWC on temperature for a given ice crystal category: (a) bullet rosette, (b) snowflake, (c) plate and (d) column habits.....	34
13.	Cloud Particle Imaging (CPI) probe images from the 23 May 2011 MC3E event.....	37
14.	(a) ARM SGP adjusted KAZR reflectivity, radar-retrieved (b) r_e and (c) IWC , with modified gamma size distribution and $a=2.0$ using bullet rosette σ - D relationship.	39
15.	The 1-min averages of (a) ARM SGP adjusted KAZR reflectivity, (b) radar-retrieved r_e (black lines) and (c) IWC (black lines) with corresponding aircraft derived r_e and IWC values (filled red circles) from 2DC and HVPS measurements at the same altitudes (~ 7.6 km) as radar retrievals.....	42
16.	Comparisons between the retrieved (b) r_e and (c) IWC using the mean N_t value of 47 L^{-1} (solid lines) and in-situ measured time-series N_t values (dashed lines) using (a) 1-min averaged adjusted KAZR reflectivity.....	45
17.	Comparisons between the aircraft calculated using 11 kinds of ice habits σ information (same as Fig. 6) from DDA and aircraft measured PSD and the adjusted KAZR reflectivity (black line) in (a) Leg 1 and (b) Leg 2.....	46
18.	The DOE ARM KAZR derived CTHs (1-hour average) and matched GOES derived CTHs ($1^\circ \times 1^\circ$ grid box, diamonds) for the DCSs over the ARM SGP site during the MC3E.....	48
19.	As in Fig. 17, except scatterplots for all four cases during MC3E.....	48
20.	(a) ARM SGP adjusted KAZR reflectivity, (b) radar-retrieved D_e assuming hexagonal columns habits and (c) D_e assuming bullet rosette habits.....	50
21.	As in Fig. 13, except for at temperatures around -40°C	51

22.	GOES and ARM retrieved D_e averaged at different reflectivity thresholds. The mean value of GOES retrieved D_e is 81 μm	52
23.	Comparisons between KAZR-retrieved (with bullet rosettes ice habits) and GOES retrieved D_e values during the MC3E.....	53
24.	Comparison between the 0 dBZ height and the GOES retrieved effective cloud height H_{eff}	54
25.	As in Fig. 6 except for 10 cm wavelength and $-25\text{ }^\circ\text{C}$	57
26.	The 1-min averages of (a) NEXRAD reflectivity along aircraft track, (b) radar-retrieved r_e (black lines) and (c) IWC (black lines) with corresponding aircraft derived r_e (filled red circles) and IWC values (filled blue circles) from 2DC and HVPS measurements at the same altitudes ($\sim 7.6\text{ km}$) as radar retrievals.....	58
27.	Comparison between KAZR-retrieved (with hexagonal column and bullet rosette ice habits) and GOES-retrieved (during both daytime and nighttime) D_e on 20 May 2011	60

LIST OF TABLES

Table	Page
1. Mean values of variance parameter X for different a values from 0.05 to 3.0.	16
2. Characteristics of 11 non-crystal ice particles defined in the DDA method and regrouped into four categories of ice crystal habits in this study.....	21
3. Comparison of calculated mean reflectivity values using parameterized bullet rosette σ -D relationship and DDA database results.....	23
4. Retrieved r_e results at different α and N_t values.....	32
5. Retrieved IWC results at different α and N_t values.....	33
6. Dependence of radar reflectivity-retrieved r_e and IWC on radar reflectivity with a fixed value of $N_t=50$ #/L and $\alpha=2.0$ for four ice crystal habits: bullet rosette, snowflake, plate and column.....	35
7. Comparison of ice cloud microphysical properties derived from aircraft measurements and retrieved from adjusted KAZR reflectivity	43
8. Comparison of ice cloud microphysical properties derived from aircraft measurements and retrieved from adjusted KAZR reflectivity using the mean N_t value and in-situ time-series N_t values.	45
9. Mean, mean difference, RMSE, and correlation coefficient values of ARM and GOES retrieved D_e	53
10. Comparison of ice cloud microphysical properties derived from aircraft measurements and retrieved from NEXRAD reflectivity.....	59

ACKNOWLEDGEMENTS

I would like to thank my advisors, Drs. Xiquan Dong and Baike Xi for providing me the opportunity to work on this research and for his guidance and support. Additionally, I would like to thank the remainder of my advisement committee, Dr. Mark Anthony Askelson for their comments, suggestions, and expert input into this thesis. I appreciate the assistance of Scott Giangrande and Tami Toto from BNL for providing the adjusted KAZR data. Thanks to Jingyu Wang for providing the in situ data and NEXRAD CSA results.

My grateful thanks are also extended to the members of my research group, as well as the remaining faculty, staff, and graduate students of the Department of Atmospheric Sciences at the University of North Dakota. Last but not least, I want to thank my parents for always being supportive to my life and my decisions.

The data were obtained from the Atmospheric Radiation Measurement (ARM) Program sponsored by the U.S. Department of Energy (DOE) Office of Energy Research, Office of Health and Environmental Research, Environmental Sciences Division. This study was primarily supported by DOE ASR project at University of North Dakota with award number DE-SC0008468 and the NASA CERES project at University of North Dakota project under Grant NNX10AI05G.

ABSTRACT

This study presents an algorithm for retrieving the Deep Convective Systems (DCSs) ice cloud microphysical properties using the DOE Atmospheric Radiation Measurement (ARM) Ka-band Zenith Radar (KAZR) reflectivity during the Midlatitude Continental Convective Clouds Experiment (MC3E) at the ARM Southern Great Plain (SGP) site (36° 36' 18.0" N, 97° 29' 6.0" W) from April-June 2011. It is a challenge to retrieve DCS ice cloud microphysical properties due to the attenuation of cloud radar reflectivity, unknown particle size distributions (PSDs), and the bulk habit of the ice particles within the sample volume. To address the most pronounced of these radar limitations, the original KAZR reflectivity measurements have been adjusted using data collected with both a collocated unattenuated 915-MHz profiling radar system UHF ARM Zenith Radar (UAZR) and a Joss-Waldvogel impact disdrometer (JWD). Additionally, aircraft in-situ measurements provide PSDs and best-estimate ice water content (*IWC*) for validating radar retrievals. With the aid of the scattering database (SCATDB), the relationships between backscatter cross section (σ) and particle dimension (*D*) are parameterized for four ice crystal habits (bullet rosettes, snowflakes, columns and plates).

The DCS ice cloud *IWC* and effective radius (r_e) on 20 May 2011 during the MC3E have been retrieved from adjusted KAZR reflectivity assuming a modified gamma distribution with size shape $\alpha=2$, and a bullet rosette σ -*D* relationship. The averaged *IWC* and r_e from

radar retrievals over the stratiform rain (SR) region of the DCS are 0.34 g m^{-3} and $338 \text{ }\mu\text{m}$, in excellent agreement with aircraft in-situ measured IWC (0.34 g m^{-3}) and r_e ($337 \text{ }\mu\text{m}$). Over the anvil cloud (AC) region, the retrieved and measured $IWCs$ are 0.18 g m^{-3} and 0.23 g m^{-3} and their respective r_e values are $250 \text{ }\mu\text{m}$ and $305 \text{ }\mu\text{m}$. The radar retrieved r_e and IWC can increase to $283 \text{ }\mu\text{m}$ and 0.23 g m^{-3} if a 2 dB uncertainty is added to the adjusted KAZR reflectivity over the AC region, following the sensitivities of 13%/2 dB in r_e and 26%/2 dB in IWC .

These retrieval results are also compared with Geostationary Operational Environmental Satellite (GOES) retrieved cloud effective diameter (D_e) during MC3E. In addition to the spatially averaged GOES retrievals within a $1^\circ \times 1^\circ$ grid box centered over the ARM SGP site and the temporally averaged ARM retrievals within 1 hr (± 0.5 hr GOES image), the ARM-retrieved D_e values were also averaged from cloud top down to where the reflectivity is around 0 dBZ to best match the GOES retrievals. During daytime, GOES retrieved D_e , on average, agrees with the ARM retrievals within $\sim 25 \text{ }\mu\text{m}$ despite the vastly different temporal and spatial resolutions of vertically pointing ground-based radar and cloud-top-viewing satellite instruments. GOES retrieved cloud top heights (CTHs) are also compared with ARM KAZR reflectivity profiles, having an excellent agreement with differences of $\sim 0.2 \text{ km}$.

CHAPTER I

INTRODUCTION

Accurate representation of convective processes in numerical models is necessary for improving current and future simulations of the Earth's climate system. However, lack of understandings of the detailed cloud properties of convective systems is an important issue to prevent and accurate parameterization, especially for cloud microphysical properties. These cloud properties, including height, effective particle size, and condensed/frozen water path, are the key parameters needed to link atmospheric radiation and hydrological budgets (Dong et al., 2008; Minnis et al., 2011). Although some of these properties are directly and reliably measured using research aircraft, most aircraft cannot be operated under all convective conditions (safely) and therefore the collected aircraft in-situ measurements represent very limited convective storm sampling volumes (both spatially and temporally). Thus, it is beneficial to develop targeted retrievals from long-term observations to assist in filling gaps of the ice cloud microphysical properties within convective systems.

Quite often, in model simulations, deep convective systems DCSs can be partitioned according to bulk precipitation and/or cloud regimes to assist in evaluating dominant microphysical behaviors within each region, or can be partitioned in the context of other bulk latent heating profiling considerations (e.g., Tao et al., 1990; Schumacher et al., 2004). Based on radar measurements, a DCS can be classified into convective core (CC) regions

(heavy rain), stratiform rain (SR) regions (moderate-light rain), and anvil cloud (AC) regions (little or no rain) (Feng et al., 2011). The SR and AC regions of DCSs produce about 10 times the spatial coverage of the CC regions (Feng et al., 2011). The upper portions of SR and AC regions are mainly ice particles, and these ice layers dominate the DCS radiation budget (Wang et al., 2005; Feng et al., 2012). To better estimate the Earth's radiation budget and improve climate forecast capabilities, accurate vertical distributions and temporal variations of the ice cloud microphysical properties in the SR and AC regions of DCSs are needed.

Unlike single-layer thin cirrus clouds, deep convective clouds, except their thin anvil regions, are optically thick. Various retrieval algorithms for single-layer thin cirrus cloud microphysical properties have been developed (e.g. Mace et al., 1998 and 2002; Wang and Sassen, 2002; Deng and Mace, 2006; Comstock et al., 2007), which introduced different methods to retrieve the microphysical properties and can help with development of a new algorithm for retrieval of DCS ice cloud microphysical properties. The retrieval algorithms for single-layer thin cirrus clouds depend upon instrument type—for example, radiometer, lidar and radar. Each instrument has its own advantages and disadvantages, so combining various measurements can exploit the natural synergy among the measurements. Combining radiometer and/or lidar observations with radar observations offers considerable insights into ice cloud microphysics (e.g. Mace et al., 1998; Matrosov, 1999; Donovan and Van Lammeren, 2001; Matrosov et al., 2002; Wang and Sassen, 2002; Comstock et al., 2007; Delanoë and Hogan, 2008). However, these remote sensing approaches are limited by either lidar attenuation or infrared saturation in optically thick DCS clouds. Additionally, most of these algorithms only work in the regions where

clouds are detected by all instruments, which limit their application. Thus, retrieval approaches relying solely on the use of Doppler radar reflectivity and velocity measurements have been suggested (e.g. Mace et al., 2002; Matrosov et al., 2002). Without the issues of lidar attenuation and infrared saturation, the radar-only algorithms can be used to retrieve cloud properties in multilayered and optically thick clouds (Comstock et al., 2007). However, the contribution of ice crystal fall speed to the measured mean Doppler velocity must be separated from the air motion before applying the Doppler velocity-based retrieval. In the Doppler-velocity-based retrieval algorithms, one must assume that the residual air motions should be much less than the sedimentation speeds of the particles that contribute mostly to the radar Doppler velocity measurements after proper time averaging (usually on the order of several hours). This approach can only be used to estimate the particle fall velocities for clouds that do not have strong updrafts/downdrafts. Owing to the strong air turbulence and no reliable estimate of the air turbulence within a DCS, this approach cannot be applied in microphysical property retrievals for DCSs. Thus, the intent is to develop a new retrieval approach utilizing radar reflectivity only.

As discussed above, although many algorithms have been developed for single-layer optically thin cirrus clouds, studies that focused on retrieving cloud microphysical properties from optically thick DCSs are limited. To study the microphysical properties of convectively generated optically thick cirrus clouds, the National Aeronautics and Space Administration (NASA) conducted a field experiment named the Cirrus Regional Study of Tropical Anvils and Cirrus Layers (CRYSTAL) Florida Area Cirrus Experiment (FACE). During CRYSTAL-FACE, more than 10 convectively generated cirrus clouds

were sampled using the University of North Dakota (UND) research aircraft and their microphysical properties were retrieved from 9.6 and 94 GHz radars reflectivity measurements aboard the high-altitude ER-2 aircraft (Heymsfield et al., 2007). Heymsfield et al. (2005) calculated *IWCs* from a total of 5000 PSDs, and developed an empirical relationship between radar reflectivity and *IWC* based on radar reflectivities at 9.6 and 94 GHz frequencies. Wang et al. (2005) developed an algorithm to retrieve optically thick ice cloud microphysical properties using 9.6 and 94 GHz radar measurements aboard the high-altitude ER-2 aircraft, and fitted both the ratios of 9.6 GHz radar reflectivity to *IWC* and particle size as function of Dual Wavelength Ratio (DWR). In contrast to ground-based radar measurements, airborne radar measurements avoid attenuation from precipitation associated with DCSs. However, aircraft cannot be used to obtain continuous and long-term radar observations.

To investigate formation-dissipation processes and microphysical properties of continental DCSs, a field campaign was conducted through the joint support of the Department of Energy (DOE) Atmospheric Radiation Measurement (ARM) and the NASA Global Precipitation Measurement (GPM) mission. The field campaign named the Midlatitude Continental Convective Clouds Experiment (MC3E) was conducted at the ARM Southern Great Plains (SGP) site from April-June 2011 (Jensen et al., 2010). The MC3E was a highly successful field campaign with six deep convective cases sampled using the UND Citation II research aircraft and observed using multiple ground-based sensors. The best-estimate PSDs and *IWCs* of the ice-phase layer of the DCSs during the MC3E have been provided using a combination of a two-dimensional cloud probe (2DC), a High Volume Precipitation Spectrometer (HVPS), Nevzorov hot-wire total water

content (*TWC*) probe, and a King hot wire *LWC* probe. In addition to the aircraft measurements, the adjusted Ka-band ARM Zenith Radar (KAZR) reflectivity is also a motivation to develop a new algorithm for retrieving DCS ice cloud microphysical properties in this study. The ARM SGP KAZR radar reflectivity measurements are normally attenuated during the heavy precipitation events. Thus, its measurements are highly questionable under heavy precipitation conditions. To address this issue, multiple ground-based precipitation sensors, including longer-wavelength unattenuated profiling radars, were collocated with KAZR during the MC3E campaign (e.g., Tridon et al., 2013, Giangrande et al., 2013). The adjusted KAZR reflectivity has provided a solid basis for developing a reliable retrieval algorithm in this study. The aircraft in-situ measurements during the MC3E will provide a validation data source for newly retrieved DCSs ice cloud microphysical properties. With the newly developed retrieval method described in this study, GOES satellite retrieved cloud-top heights (CTHs) and particle size during the MC3E are compared with ARM radar observations and retrievals.

The NASA's Clouds and Earth's Radiant Energy System (CERES) project has provided long-term global estimates of the Earth's broadband radiation budget and retrieved cloud properties that produce consistent radiative fluxes from the surface to the top of the atmosphere (TOA) (Wielicki et al., 1998; Minnis et al., 2011a). A climate data record of the CERES surface and TOA radiative fluxes with collocated cloud properties is a valuable dataset for investigating the role clouds play in the radiative balance of the climate system (Wielicki et al., 1998). These products are designed to improve understanding of cloud-radiation interactions and to help answer crucial climate questions.

The NASA-Langley cloud working group produced cloud and radiation products using the Visible Infrared Solar-infrared Split-Window Technique (VISST) and Solar-infrared Infrared Split-Window Technique (SIST) based on long-term satellite observations. GOES channels are used in these techniques to detect clouds and retrieve cloud properties. It is important to validate these satellite retrievals using both ground-based data and aircraft in-situ measurements and find a meaningful way to interpret these results (Dong et al. 2002 and 2008; Yost et al., 2010). However, due to lack of reliable radar observations and retrievals, GOES retrieved cloud properties have not yet been fully evaluated. In addition, Minnis et al. (2008) improved the estimation of the physical cloud top heights (CTHs) for optically thick ice clouds using a combination of Cloud-Aerosol Lidar and Infrared Pathfinder Satellite Observations (CALIPSO) and Aqua Moderate Resolution Imaging Spectroradiometer (MODIS) data. However, Sherowd et al. (2004) demonstrated that deep convective clouds do not have sharply defined boundaries in the IR spectrum, thus it has a significant biases in satellite retrieval. Thus, comparison of satellite retrieved CTH is also performed in this study.

In a series of studies, algorithms for retrieving DCS ice, mixed-phase and liquid cloud microphysical properties will be developed from multiple ground-based measurements during the MCE3 field campaign, with aircraft in-situ measurements used as a validation source. The first part of this study focuses on DCS ice cloud microphysical properties. Section 2 presents the datasets and retrieval methodology. Section 3 discusses the results for the DCS case of 20 May 2011 and the application of retrieval algorithm: comparing GOES retrievals using ARM measurements and retrievals

collected/performed during MC3E. Finally, a summary and description of future work is provided in section 4.

CHAPTER II

DATA AND METHODOLOGY

Data

One of the MC3E goals was to advance understanding of cloud microphysical properties of DCSs using multi-platform observations, such as those from the ground-based ARM cloud radar KAZR, microwave radiometers (MWRs), JWDs, and radiosonde soundings, with the help of additional ground-based radars, precipitation sensors, and the UND Citation II research aircraft in-situ measurements (Jensen et al., 2010). As previously mentioned, six DCS cases were observed during the MC3E campaign. However, during most of the flights, the aircraft flew far away from the ARM SGP site/cloud radar KAZR location. The distance between aircraft track and the SGP site/KAZR location was commonly greater than 30 km. At this distance, it is hard to ensure that the same DCS cloud microphysical properties were measured with the aircraft and KAZR. Fortunately, the UND Citation aircraft flew mostly within 20 km of the ARM SGP central facility during the 20 May 2011 MC3E case. In addition, during this flight, there are two different kinds of legs, one was in the SR region of DCS, and another was in the AC region of DCS. The aircraft in-situ measurements from SR and AC regions of the same DCS is comparable. Thus, this case was chosen as a starting point for developing the retrieval algorithm. Early in the morning of 20 May 2011, an intense north-to-south oriented convective line moved over the ARM SGP site and was

extensively sampled using ground-based instruments. Shortly after, the SR and AC regions of the DCS were sampled using the UND Citation II near the ARM SGP site. This classic DCS case on 20 May 2011 became known as the “Dream Scenario”, and represents one of the best examples of coordinated measurements obtained throughout the entire MC3E campaign—for both observational and modeling communities (Petersen and Jensen, 2012; Tao et al., 2013).

ARM Ground-based Observations

KAZR is a profiling Doppler radar that operates at a frequency of approximately 35 GHz (8.6 mm wavelength/ Ka band) and has excellent sensitivity for detecting cloud droplets, ice crystals and light drizzle. This radar can be significantly attenuated in heavier precipitation and can be of questionable use for retrievals even for non-precipitating DCS cases including those having large liquid water paths (*LWPs*) (Lhermitte, 1990; Moran et al., 1998; Kollias et al., 2007; Dong et al., 2008; Feng et al., 2009). For example, *Feng et al.* (2009) found that specific attenuation is a function of *LWC* and the hydrometeor temperature. Figure 1a shows the JWD-measured surface rain rate and MWR-retrieved cloud *LWP* at the ARM SGP site on 20 May 2011. The cloud *LWP* is retrieved from interpolated radiosonde profiles using optimal estimation in an iterative scheme (Turner et al., 2004). The surface rain rate is measured from the JWD at the ARM SGP Central Facility in close proximity to the KAZR. As shown in Fig. 1a, the maximum rain rate reached up to 100 mm hr⁻¹ during the peak period between 10:30-11:00 UTC, and cloud *LWPs* are as large as 5 kg m⁻² during the period from 09:00 – 16:00 UTC. The attenuated ARM KAZR product Active Remote Sensing of Clouds

(ARSCL, e.g. Clothiaux et al., 2000) reflectivities are shown in Fig. 1b, with a clear attenuation band during the period 10:30-11:00 UTC.

Although KAZR reflectivities are attenuated in rain during DCS conditions, these measurements may be improved significantly when coupled with unattenuated profiling references (e.g., Matrasov, 2005; Feng et al., 2009 and 2014). During the MC3E, the KAZR was collocated with the unattenuated 915 MHz profiler UAZR and adjusted using UAZR measurements and a JWD (e.g., Tridon et al., 2013; Giangrande et al., 2013). The KAZR was cross-calibrated against available surface disdrometers, ARM and NASA campaign radars, and nearby Next Generation Weather Radar (NEXRAD) data to promote a relative calibration to within several dB (shown later). By combining reflectivity and Doppler velocity data from both KAZR and UAZR as well as from a surface disdrometer, a merging was performed to better estimate bulk KAZR reflectivity offsets aloft and to adjust KAZR measurements for well-known system calibration biases, attenuation in rain, and additional wet-radome effects. Manual checks of individual profiles were performed to ensure modest merging success near the surface. These products are assumed to be sufficient for the use of adjusted KAZR reflectivity as a foundation for successful retrieval of DCS ice cloud microphysical properties in a manner similar to top-down aircraft studies (e.g. Heymsfield et al., 2002a and 2002b). The adjusted KAZR reflectivities used in the retrieval (Fig. 1c) are noticeably higher than the original KAZR ARSCL reflectivities (Fig. 1b) for this event. The isotherms in Fig. 1b and 1c are estimated from ARM merged soundings that were generated from a combination of observations from radiosonde soundings, MWR, surface meteorological

instruments, and European Centre for Medium Range Weather Forecasts (ECMWF) model output.

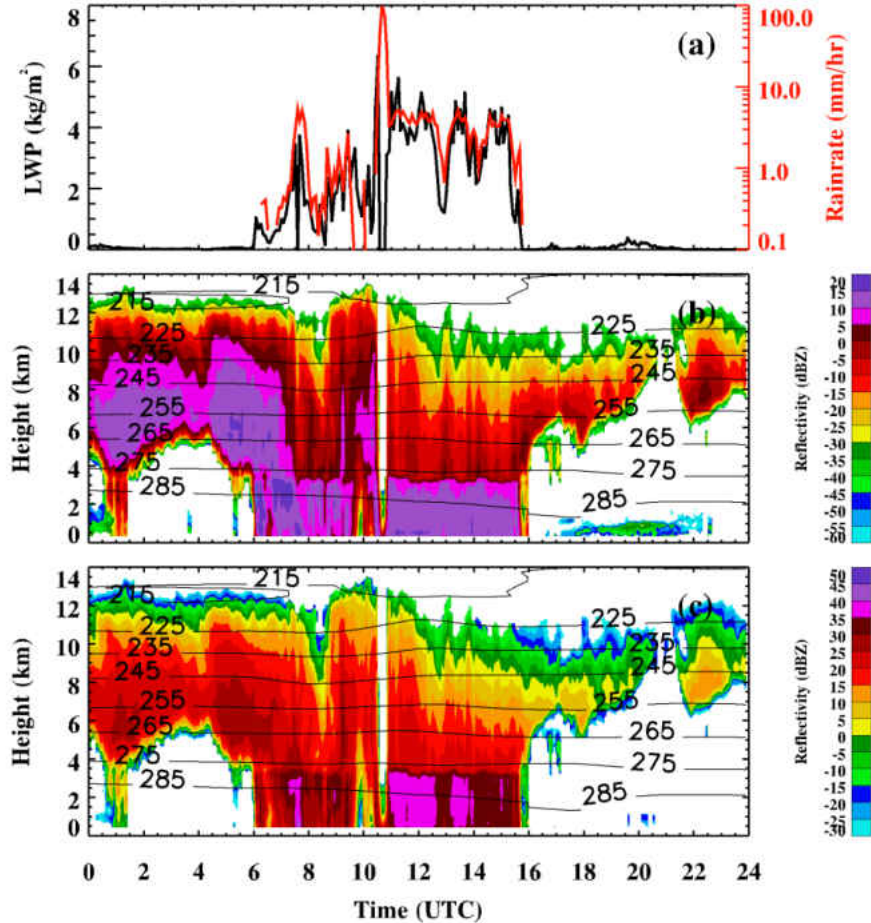


Figure 1. (a) Joss-Waldvogel impact disdrometer (JWD)-measured rain rate (red line) and MWR-retrieved cloud LWP (black line), (b) ARM SGP KAZR ARSCL reflectivity (above ground level, AGL) and (c) Combined ARM SGP UAZR calibrated, JWD adjusted KAZR reflectivity. Temperature contours (black lines) are from ARM Merged-Sounding VAP on 20 May 2011.

Aircraft In-situ Measurements

The UND Citation II research aircraft was one of the primary research aircraft deployed during the ARM MC3E field campaign, and was fully equipped for cloud physics research. The onboard probes used in this study consist of a 2DC, HVPS, Nevzorov hot wire *TWC* probe, and the King hot wire *LWC* probe. For example, the

Droplet Measurement Technologies (DMT) Cloud Droplet Probe (CDP) can be used to measure cloud particles smaller than 50 μm , the 2DC probe can be used to measure a range of particle sizes from 30 to 3000 μm , and the HVPS probe has a broad range between 300 and 30,000 μm . In the following discussion, the entire spectrum is constructed using only a combination of 2DC and HVPS measurements because this study mainly focuses on the DCS ice cloud microphysical properties, for which the CDP probe measurements are not overly useful due to associated large uncertainties when measuring irregularly-shaped ice crystals and due to its limited size-sensitivity range ($D < 50 \mu\text{m}$). In addition, for the overlapping spectrum region measured with both the 2DC and HVPS, HVPS measurements were used to reduce uncertainty due to the fact that with the 2DC one can only reconstruct the images of particles larger than 1000 μm (McFarquhar et al., 2007). Moreover, the first three channels of the 2DC ($D < \sim 90 \mu\text{m}$) were discarded due to artifacts associated with the shattering of ice crystals and collision-induced breakup of raindrops (McFarquhar et al., 2004). Both the 2DC and HVPS probes were well calibrated and functioning well before the field campaign. For cloud water content measurement, the Citation II was equipped with a Nevzorov hot wire *LWC/TWC* probe (CWCM-U2) (Korolev et al., 1998) and a Particle Measurement System (PMS) King hot-wire *LWC* probe (King et al., 1978 and 1985). In this study, the PSDs are assumed to have shapes given by the modified gamma distribution, and the *IWC* and r_e values that are calculated from aircraft measurements are used to validate the radar-reflectivity-based retrievals.

Figure 2a shows the aircraft flight trajectory from 13:05:39 UTC to 17:02:04 UTC on 20 May 2011. As illustrated in Fig. 2, the UND Citation aircraft flew mostly within 20

km of the ARM SGP central facility, especially for the two time periods used in this study: Leg 1 (14:15-14:32 UTC at ~ 7.6 km) over the SR region of the DCS and Leg 2 (16:07-16:16 UTC at ~ 7.6 km) over the AC region of DCS.

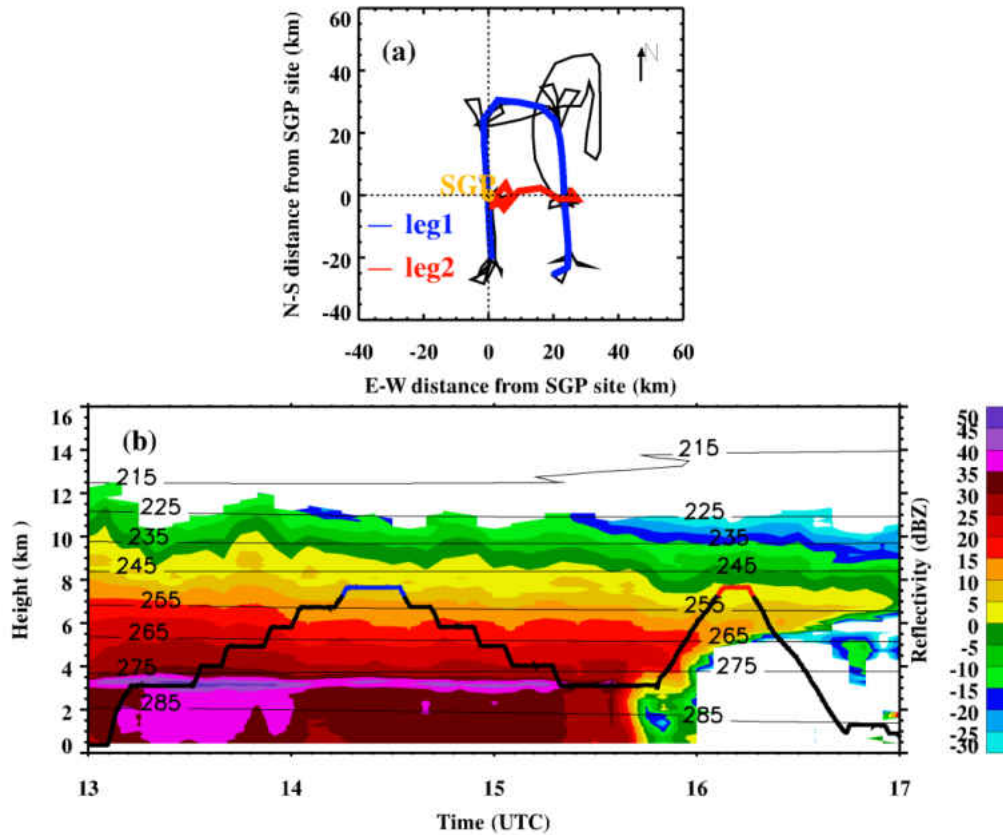


Figure 2. (a) UND Citation II aircraft flight patterns (black lines) over the ARM SGP site during 20 May 2011. (b) ARM SGP corrected KAZR reflectivity with aircraft flight trajectory (thick black line with blue Leg1 and red Leg2) and temperature contours (thin black lines) on 20 May 2011.

To provide additional details about microphysical properties measurements from the aircraft at times during the two legs on 20 May 2011, a series of 2-min averaged PSDs derived from a combination of 2DC and HVPS measurements (filled circles) are shown in Fig. 3. Figure 3 also demonstrates the modified gamma function with different shape

parameter α values (color lines). The modified gamma function $N(D)$ can be expressed as

$$N(D) = N_x e^{\alpha} \left(\frac{D}{D_x}\right)^{\alpha} \exp\left(-\alpha \frac{D}{D_x}\right), \quad (1)$$

where N_x is the number of particles per unit volume per unit length at the size D_x where the function $N(D)$ is a maximum (Gossard, 1994; Mace et al., 1998; Wang and Sassen, 2002; Deng et al., 2006). The α parameter denotes the breadth of the spectrum; the larger the magnitude of α , the narrower the spectrum becomes. For any given 2-min averaged particle spectra, it is easy to find the maximum of the number concentration and corresponding D . We assume this identified maximum number concentration value as N_x , and the corresponding particle size value as D_x . Then, with given N_x and D_x , α values are varied (colored lines), based on (1), and a PSD plot can be generated (Fig. 3).

Although it is clear in Fig. 3 that the observed α values during Leg 1 are close to 2.0, for Leg 2, they are close to 1.5 or 1.0. A simple statistical method is used to minimize the variance parameter (X) between the calculated and observed PSDs. X is defined as

$$X = \sum W_i (\log_{10}(Y_{obs}) - \log_{10}(Y_i))^2, \quad (2)$$

where Y_i is the calculated PSD number concentration, Y_{obs} is the observed PSD number concentration, and W_i is the weighting function. Here, Gaussian weighting is used:

$$W_i = 1.0 / (\text{standard_deviation}(\log_{10}(Y_{obs})))^2. \quad (3)$$

Using the logarithm form in (2) and (3) can limit the impact of differences for small hydrometeors, for which the concentrations and, thus, differences, are expected to be much larger. In addition, the unit of reflectivity factor is dBZ, which is a logarithmic dimensionless technical unit, thus a logarithm form was used in (2) and (3). Table 1 shows the X values for different α values during the two legs. The modified gamma distribution with $\alpha=2.0$ has a minimum value of X during leg 1, while the modified

gamma distribution with $\alpha=1.5$ reaches its minimum value of X during leg 2. The retrieved r_e and IWC differences using α values of 1.5 and 2 are less than 3% and 6%, respectively. To keep the retrievals consistent, the modified gamma with $\alpha=2$ has been used in the radar retrievals. Deng and Mace (2006) developed an algorithm that uses millimeter-wavelength radar Doppler moments to retrieve single-layer cirrus cloud microphysical properties assuming a modified gamma PSD (1) with α equal to 5, which was proved to produce accurate retrievals. For single-layer cirrus clouds, the maximum particle size shown in PSD plots is around 1000 μm (800 μm in Mace et al., 2002; 1200 μm in Deng and Mace, 2006). However, for DCS ice clouds, the maximum particle size shown in Fig. 3 can be greater than 4000 μm . This result demonstrates that the DCS ice clouds have a much broader spectrum compared to a single layer cirrus clouds. Based on the physical meaning of α , the broader spectrum will lead to a smaller α value, which also supports the use of a smaller $\alpha=2.0$ value for DCS ice clouds.

$\alpha = 0.05$ $\alpha = 0.50$ $\alpha = 1.00$ $\alpha = 1.50$ $\alpha = 2.00$ $\alpha = 3.00$ • aircraft

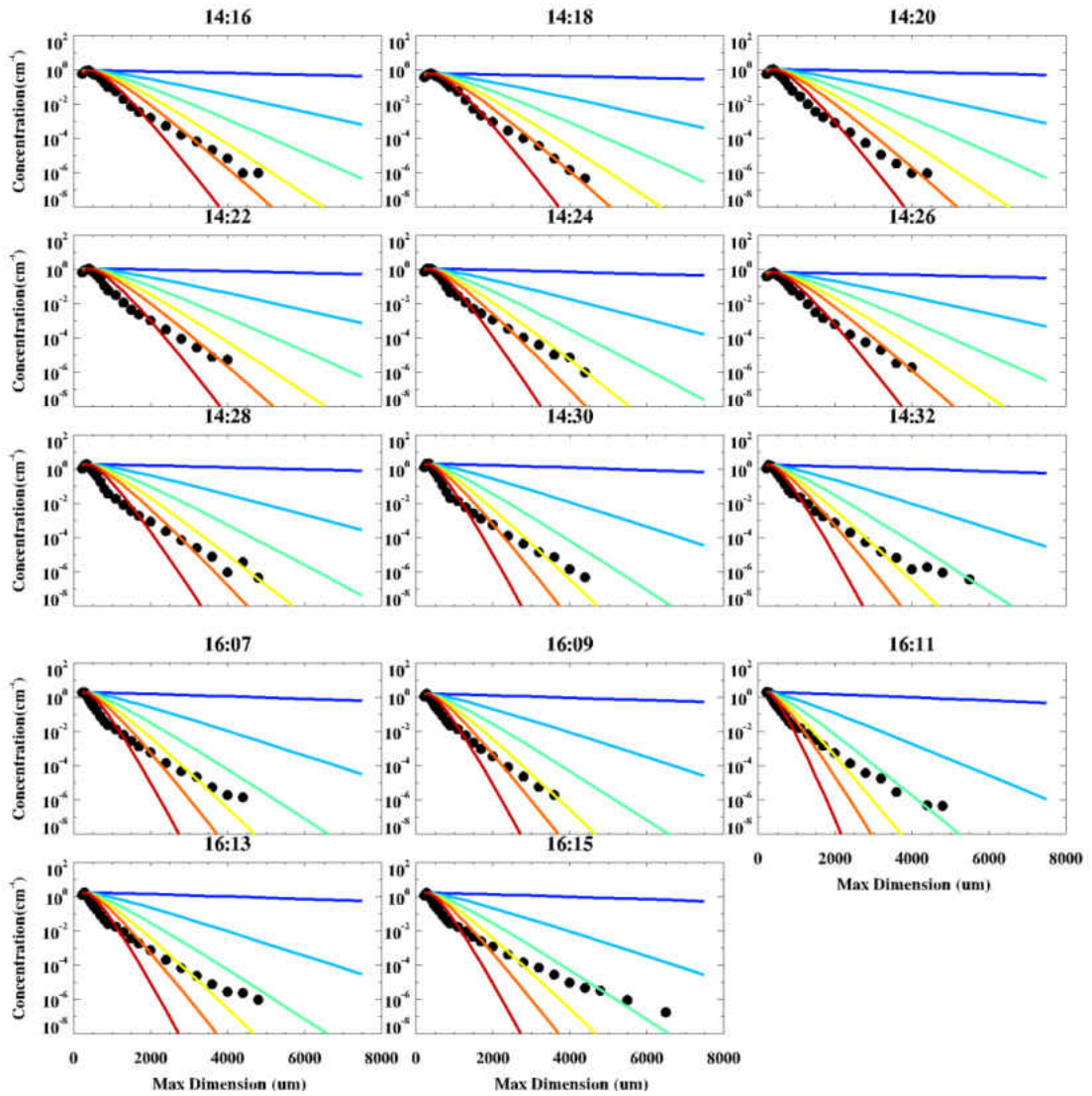


Figure 3. A series of 2-min averaged particle size distributions (PSDs) derived from a combination of 2DC (30-3,000 μm) and High Volume Precipitation Spectrometer (HVPS, 300 and 30,000 μm) (filled circle) measurements obtained with the UND Citation II Research aircraft on 20 May 2011. The modified gamma functions are plotted with different shape parameter α values (Color lines for $\alpha=0.05, 0.5, 1.0, 1.5, 2.0,$ and 3.0).

Table 1. Mean values of variance parameter X for different α values from 0.05 to 3.0

	0.05	0.5	1	1.5	2	3
Leg 1	41.5	24.4	11.5	4.9	4.6	22.8
Leg 2	49.4	22.7	7.3	6.9	21.5	95.7

Next Generation Weather Radar (NEXRAD) data

The NEXRAD is operated at a wavelength of 10 cm (S band) and is used to monitor the environment in a preprogrammed sequence of 360° azimuthal sweeps at various elevation angles. Thus, NEXRAD observations represent a close instantaneous measurement of radar reflectivity at a given elevation and azimuth angle. The NEXRAD radar dataset used in this study was obtained from the National Severe Storms Laboratory National Mosaic and Multi-Sensor Quantitative Precipitation Estimate project (Zhang et al., 2011). Feng et al. (2011) classifies a DCS into three components, CC, SR, and AC regions, using the Convective Stratiform Anvil (CSA) classification algorithm. CC is defined as strong, vertically oriented reflectivity maxima that produce intense precipitation, with contiguous (no radar reflectivity gap from echo base to echo top) echoes having tops above 6 km. SR is defined as widespread precipitation that has a weak horizontal reflectivity gradient and (at times) enhanced reflectivity near the 0 °C level (bright band), along with contiguous echoes with tops above 6 km. An AC region is defined as neither convective nor stratiform rain. Following the *Feng et al.* (2011) CSA classification, Leg 1 is in the SR region of the DCS (Fig. 4a), while Leg 2 is in the non-precipitating AC region of the DCS (Fig. 4b). The cloud temperatures for both Legs are below -20 °C, so it is reasonable to assume that cloud properties are dominated by ice particles.

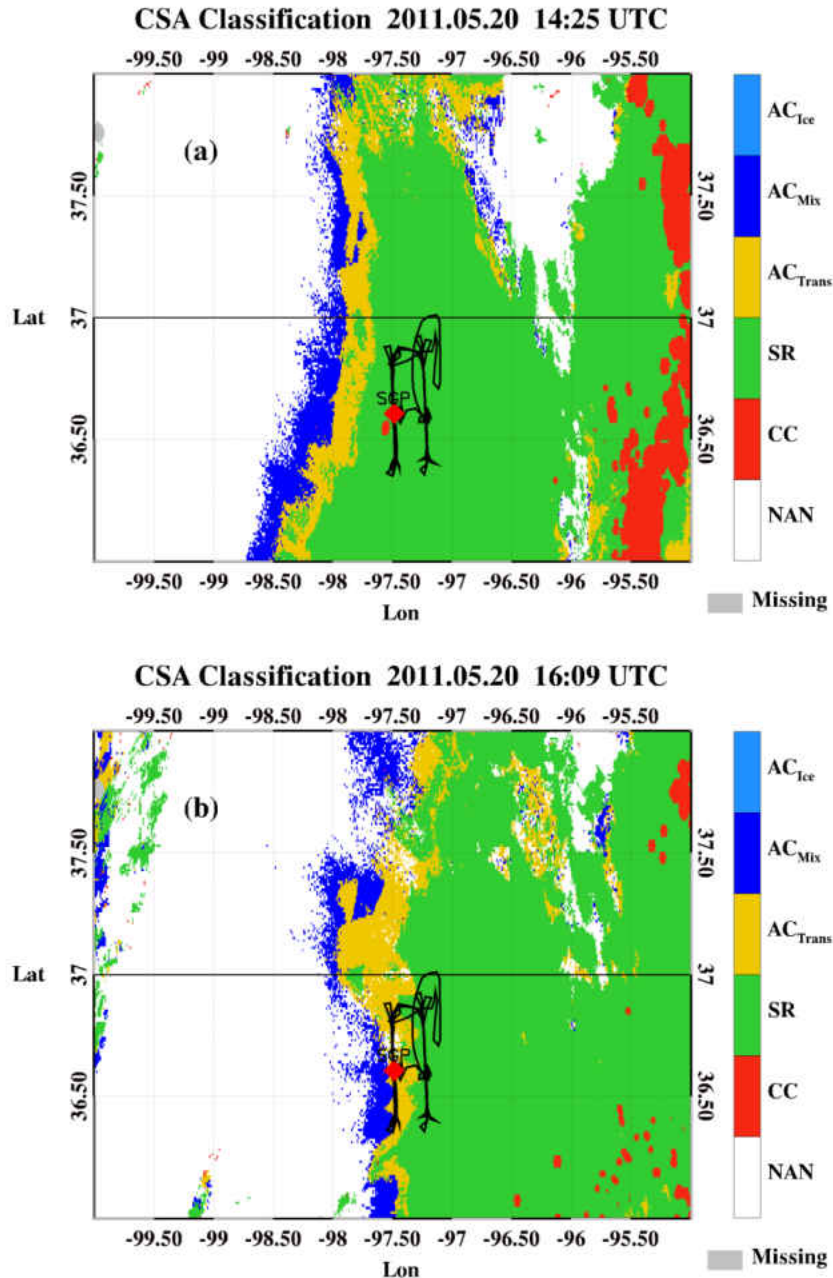


Figure 4. (a) The classified DCS components (CC-Convective Core; SR-Stratiform; AC-Anvil Cloud) based on NEXRAD observations using the Feng et al. (2011) CSA classification algorithm with the aircraft flight pattern (black lines) over the ARM SGP site (red diamond) during 14:15-14:32 UTC (Leg 1, SR region of DCS), 20 May 2011. (b) same as (a) except for the period 16:07-16:16 UTC (Leg 2, AC region of DCS).

Figure 5 shows a time series of ARM SGP adjusted KAZR reflectivity, NEXRAD cross-section reflectivity over the ARM SGP site, and differences between the two. The

KAZR reflectivities are averaged every 5 minutes to match the constraints of the NEXRAD data temporal resolution. As shown in Fig. 5a and 5b (after 16 UTC), small ice crystals in cirrus anvils cannot be detected using NEXRAD data due to their operational configuration and low sensitivity to non-precipitating particles. The reflectivity differences between adjusted KAZR and NEXRAD are -3 dB and -5 dB for Leg 1 and Leg 2, respectively. That is, the adjusted KAZR reflectivity is still a few dB less than NEXRAD observations if those were considered as one potential independent “ground truth”.

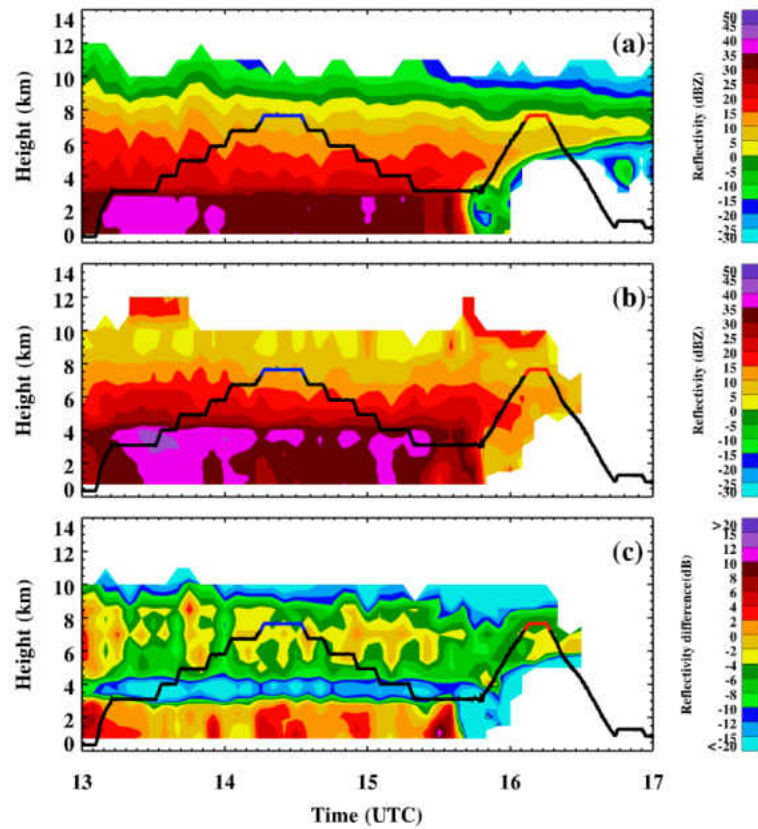


Figure 5. (a) Time series of ARM SGP adjusted KAZR reflectivity during the period 13:00-17:00 UTC when the UND aircraft data are available, (b) NEXRAD cross section at the ARM SGP site and (c) adjusted KAZR reflectivity minus NEXRAD reflectivity. Black lines are the time series of UND Citation II aircraft flight altitude with blue line for Leg 1 and red line for Leg 2.

Discrete Dipole Approximation (DDA) dataset

There are several published methods for calculating the scattering of non-spherical particles, such as the T-matrix method, finite-difference time domain method (FDTD), improved geometrical optics method (IGOM), and the discrete dipole approximation method (DDA). Ice crystal habit can significantly impact retrieved microphysical properties, so DDA methods, which are suitable for determining complex habits at cloud radar frequencies, have been widely used to calculate radar backscattering properties of non-spherical ice crystals (e.g., Schneider and Stephens, 1995; Liu and Illingworth, 1997; Aydin and Tang, 1997; Aydin and Walsh, 1999; Lemke and Quante, 1999; Okamoto, 2002; Sato and Okamoto, 2006; Hong, 2007; Liu, 2008). The scattering properties for non-spherical ice particles in this study are from the DDA dataset (Liu, 2008), which contains the scattering properties at frequencies from 15 to 340 GHz over a range of temperatures from $-40\text{ }^{\circ}\text{C}$ to $0\text{ }^{\circ}\text{C}$, particle maximum dimensions D from $50\text{ }\mu\text{m}$ to $12,500\text{ }\mu\text{m}$, and 11 particle shapes (Table 2) (the DDA database can be downloaded at <http://cirrus.met.fsu.edu/research/scatdb.html>). Usually, large amounts of computing time and memory are required to generate scattering properties of non-spherical ice particles (e.g. Kim, 2006; Hong, 2007). Thus, parameterization schemes of the scattering properties of non-spherical ice crystals have been used, and the scattering properties of non-spherical ice crystals are generally parameterized as functions of ice crystal sizes (e.g. Hong, 2007; Liu, 2008). Formulating the equations in terms of power law relations allows some flexibility for developing solutions for different particle habits (Mace et al., 2002). For this study, 11 non-spherical ice crystals from the DDA database were regrouped into four categories (bullet rosette, snowflake, plate, and column), and for each

category, a parameterization was made with radar backscatter cross section σ as a function of D in the form of

$$\sigma = sD^t, \quad (4)$$

where σ is in units of mm^2 , D is in units of mm , and s and t are fitting coefficients (Fig. 6). For example, the long columns, short columns and block columns in the DDA database have been regrouped into the column category (Table 2 and Fig. 6) in this study. Figure 6 shows 11 non-spherical σ values (at 35 GHz and $-22^\circ C$, which is the mean temperature of leg 1 and leg 2) (colored lines) and four regrouped ice crystal habits (symbols) as a function of D . The results from the four regrouped parameterizations are in agreement with those from the DDA database with correlations of 0.8 to 0.95. Fig. 7 shows the comparisons between calculated reflectivity using 4 kinds of bullet rosettes ice habits σ information from DDA database and parameterized bullet rosette σ - D relationship aircraft two flight legs. Following, table 3 provides the calculated mean reflectivity values using parameterized bullet rosette σ - D relationship and DDA database results.

Table 2. Characteristics of 11 non-crystal ice particles defined in the DDA method and regrouped into four categories of ice crystal habits in this study

shape name	Ice habit
long column	Column
short column	
block column	
thick plate	Plate
thin plate	
3-bullet rosette	Bullet rosette
4-bullet rosette	

(Table 2 cont')

5-bullet rosette	
6-bullet rosette	
sector snowflake	Snowflake
dendrite snowflake	

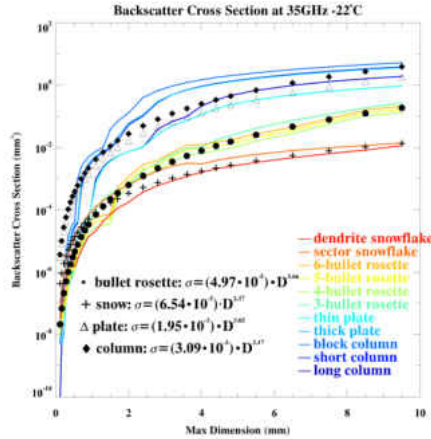


Figure 6. Radar backscatter cross section σ at 35 GHz around $-22\text{ }^{\circ}\text{C}$ as a function of maximum dimension D for 11 non-spherical ice crystals (colored lines) calculated using the discrete dipole approximation (DDA) method (Liu, 2008). Regroup 11 non-spherical ice crystals into four categories (bullet rosette, snowflake, plate, and column), and parameterize σ as a function of D for each category in this study.

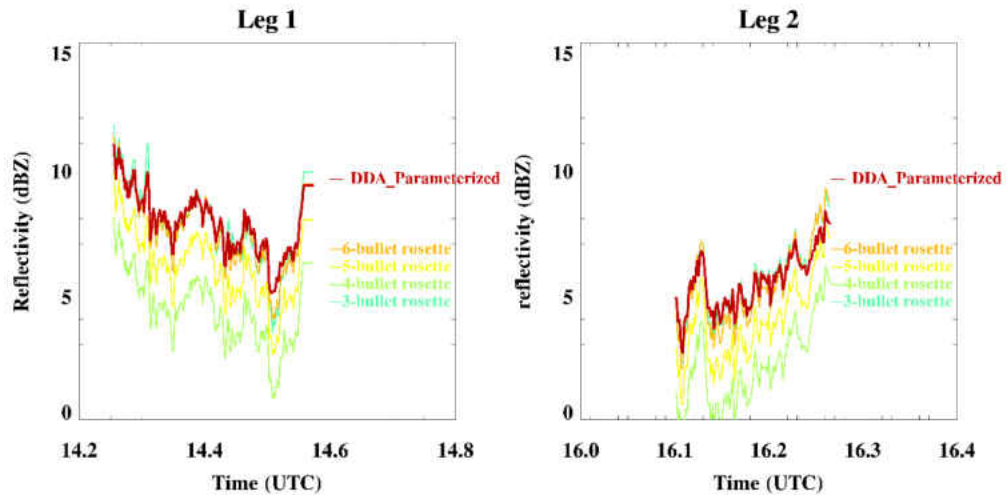


Figure 7. Comparisons between calculated reflectivity using 4 kinds of bullet rosettes ice habits σ information from DDA database and parameterized bullet rosette σ – D relationship (red lines) for (a) Leg 1 and (b) Leg 2.

Table 3. Comparison of calculated mean reflectivity values using parameterized bullet rosette σ - D relationship and DDA database results.

	Parameterized bullet rosette	3 branches bullet rosette	4 branches bullet rosette	5 branches bullet rosette	6 branches bullet rosette
Leg 1	7.8	7.8	4.4	6.2	7.6
Leg 2	6.6	7.0	3.8	5.5	6.9

On 20 May 2011, measured temperatures along the flight path are almost constant (-22 °C), therefore, the DDA parameterization should not vary with temperature. Fig. 8 shows the temperature dependent (changed every 4 °C for each panel from -20°C to -40°C) of DDA parameterization, which may be used in other cases and studies. The fitting coefficients s and t change very slightly with temperature.

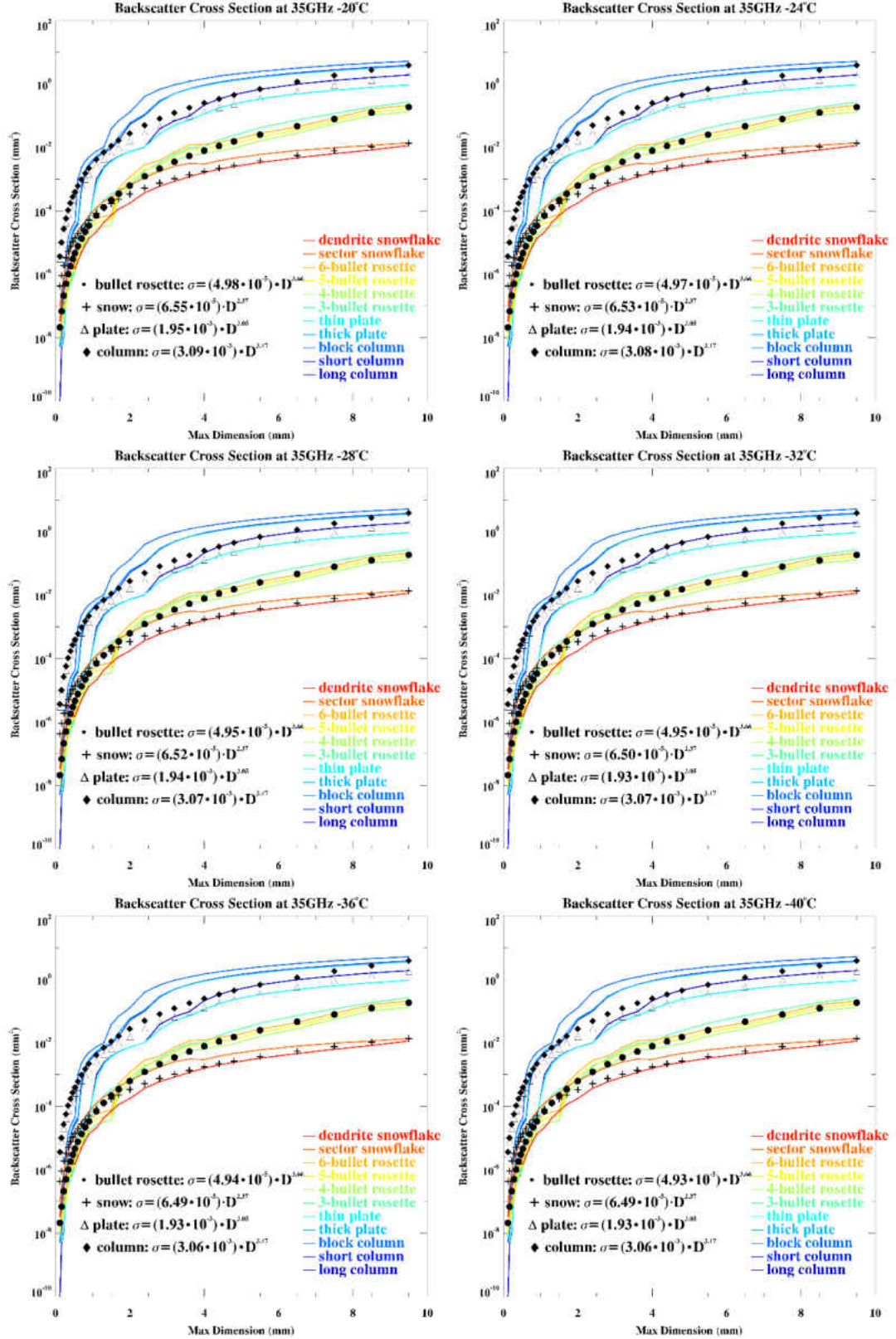


Figure 8. As in Fig. 6 but for radar backscatter cross section σ at 35 GHz from -20°C to -40°C.

Geostationary Operational Environmental Satellite (GOES) data

Cloud parameters derived from half-hourly, 4 km radiances obtained with GOES-11 (hereafter GOES) during the MC3E are compared with the ground-based observations. All satellite cloud properties in this study were derived from GOES data as described by Minnis et al. (2008, 2011). Satellite cloud retrieval data were provided by Dr. Minnis group at the NASA Langley Research Center.

During daytime, defined as solar zenith angle (SZA) $< 82^\circ$, the VISST is used to retrieve cloud D_e which relies on the solar infrared (SI: 3.9 μm) radiance. The VISST computes a set of radiances for all four wavelengths (Visible (VIS): 0.65 μm ; SI: 3.9 μm ; infrared (IR): 10.8 μm ; split-window channel (SWC): 12 μm) over a range of optical depths and effective particle sizes of ice crystals at given viewing and illumination angles and a profile of temperature and humidity. The computations use a set of cloud SI, IR, and SWC emittance parameterizations along with VIS and SI reflectance lookup tables (Minnis et al., 1998) in simplified radiative transfer models of the atmosphere (Minnis et al., 1993). The ice cloud properties are computed iteratively until the theoretical calculations of the VIS, SI, and IR channels match to the measured counterparts (Minnis et al., 2011). For the GOES retrievals, means were computed for CTH and D_e using all of the pixels within a 100 km \times 100 km box centered on the SGP central facility every 30 minutes.

VISST relies on the infrared (10.8 mm) radiance to determine cloud temperature (Minnis et al., 2011). Cloud effective temperature (T_{eff}) corresponds to the radiating center of the cloud, and is used to define the cloud effective height (H_{eff}), which is close to the infrared effective radiating height. H_{eff} is determined using the lowest altitude

where the atmosphere-corrected IR temperature matches a vertical temperature profile (Minnis et al., 2011). Rapid Update Cycle (RUC) analyses (Benjamin et al., 2004) were used to represent the vertical atmospheric temperature profile above 700 hPa, while a surface temperature-anchored lapse rate defines the temperature profile at lower altitudes as described by Minnis et al. (2011). For optically thick clouds (effective emittance exceeding 0.98, visible optical depth greater than 6), most IR radiation reaching the satellite sensor is emitted by the uppermost part of the cloud. Therefore, CTH is assumed to be close to H_{eff} for DCSs (Smith et al., 2008; Minnis et al., 2008 and 2011). Minnis et al. (2008) performed a regression using the CALIPSO derived CTH and GOES retrieved H_{eff} for even-day data only for ice clouds with effective pressures less than 500 hPa, yielding $\text{CTH}=1.041H_{\text{eff}}+1.32$ km. The linear fit between CTH and H_{eff} , applied to odd-day data, yields a difference of 0.03 ± 1.21 km and were used to estimate CTH from infrared-based H_{eff} for optically thick ice clouds.

Figure 9 shows GOES retrieved daytime cloud optical depth τ , CTH and D_e on 20 May 2011. Figure 9 demonstrates clearly that 20 May case is a strong deep convective case with large cloud optical depth, CTH and D_e values. As shown in Fig. 9 the maximum optical depth can reach up to 130, the highest CTH is around 17 km, and the retrieved D_e is ~ 60 μm . Notice that CTH has a negative correlation with D_e , that is, the higher of CTH is, the smaller of D_e will be. Satellite retrieved CTH and D_e are compared with ARM radar measurements and retrievals in this study.

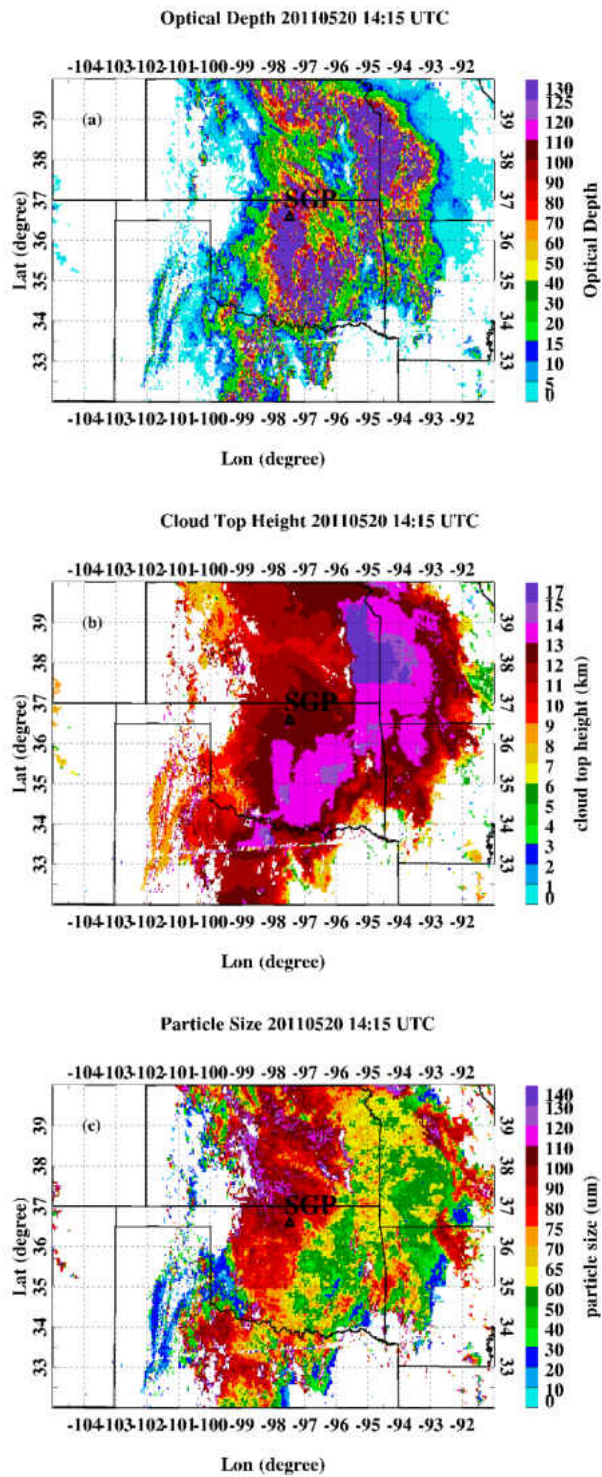


Figure 9. GOES retrieved daytime cloud optical depth τ , cloud top height CTH and particle size D_e at 14:15 UTC on 20 May, 2011.

Methodology

Retrieval Algorithm

Radar backscattering properties have been extensively used to retrieve ice cloud microphysical properties, as mentioned before. The radar reflectivity factor for ice particles Z_i (in units of $\text{mm}^6 \text{m}^{-3}$) is defined as (e.g., Donovan et al., 2004; Sato and Okamoto, 2006; Hong, 2007)

$$Z_i = \frac{\lambda^4}{\pi^5 |K_i|^2} \int_0^\infty \sigma(D) N(D) dD, \quad (5)$$

where λ is the wavelength at 35 GHz, coefficient $|K_i|$ is $|(m^2 - 1)/(m^2 + 1)|$, and m is the complex refractive index of ice crystals at 35 GHz. Radar reflectivity measurements Z_e are referred to as water equivalent reflectivity in KAZR. On the basis of Z_i , the radar reflectivity factor Z_e used in KAZR is derived by the relation (Smith, 1984; Atlas et al., 1995),

$$Z_e = Z_i \frac{|K_i|^2}{|K_w|^2}, \quad (6)$$

where $|K_w|^2$ is the dielectric factor for liquid-water and is approximately 0.88 for KAZR (Widener et al., 2012). To relate the observations of Z_e to the PSD, we combine (5) and (6) to get

$$Z_e = \frac{\lambda^4}{\pi^5 |K_w|^2} \int_0^\infty \sigma(D) N(D) dD. \quad (7)$$

Thus, using (1) and (4), (7) can be expressed as,

$$Z_e = \frac{\lambda^4}{\pi^5 |K_w|^2} \cdot s \cdot N_x e^\alpha \cdot D_x^{t+1} \cdot \frac{\Gamma(t+\alpha+1)}{\alpha^{t+\alpha+1}}, \quad (8)$$

where Γ is the gamma function [$\Gamma(z) = \int_0^\infty t^{z-1} e^{-t} dt$]. Other parameters of interest can be derived similarly. For instance, the total number concentration N_t can be written as

$$N_t = \int_0^\infty N(D) dD = N_x e^\alpha D_x \frac{\Gamma(\alpha+1)}{\alpha^{\alpha+1}}, \quad (9)$$

and r_e is defined in terms of the total volume of the distribution to the total area (Parol et al., 1991; Mace et al., 1998),

$$r_e = \frac{1}{2} \frac{\int_0^\infty D^3 N(D) dD}{\int_0^\infty D^2 N(D) dD} = \frac{1}{2} D_x \frac{\alpha+3}{\alpha}. \quad (10)$$

Combined with (9) and (10), N_x and D_x in (8) can be expressed as functions of r_e and N_t .

Then, (8) can be written as

$$Z_e = \frac{\lambda^4}{\pi^5 |K_w|^2} \cdot N_t \cdot s \cdot (2 \cdot r_e)^t \cdot \frac{\Gamma(t+\alpha+1)}{\Gamma(\alpha+1)(3+\alpha)^t}. \quad (11)$$

Solving for r_e in (11) produces

$$r_e = \frac{1}{2} \left[Z_e \cdot \left(\frac{\pi^5 |K_w|^2}{\lambda^4} \right) \cdot \frac{1}{N_t} \cdot \frac{\Gamma(\alpha+1)(3+\alpha)^t}{\Gamma(t+\alpha+1)} \cdot \frac{1}{s} \right]^{(1/t)}. \quad (12)$$

Equation (12) is used to retrieve r_e based on adjusted KAZR reflectivity in this study.

It is easily seen that the retrieved r_e is a function of N_t , Z_e , the PSD α value, and DDA parameterization coefficient values related to ice habits.

IWC can be derived by integrating the individual particle mass over the PSD,

$$IWC = \int_0^\infty M(D) N(D) dD. \quad (13)$$

For the modified gamma PSD considered here, by using a mass dimension power-law relationship

$$M(D) = p D^q, \quad (14)$$

where p and q are the power-law parameters, the *IWC* can be estimated as

$$IWC = \int_0^\infty p D^q N_x e^\alpha \left(\frac{D}{D_x} \right)^\alpha \exp\left(-\alpha \frac{D}{D_x}\right) dD. \quad (15)$$

Combining (9) and (10) with (15), IWC can similarly be expressed as

$$IWC = N_t \cdot p \cdot \left(\frac{2 \cdot r_e \cdot \Gamma(\alpha+3)}{\Gamma(\alpha+4)} \right)^q \cdot \frac{\Gamma(\alpha+q+1)}{\Gamma(\alpha+1)}. \quad (16)$$

Thus, by substituting the r_e expression in (12) into (16) one can estimate IWC from Z_e using

$$IWC = p \cdot N_t^{(1-q/t)} \cdot \left[Z_e \cdot \left(\frac{\pi^5 |K_w|^2}{\lambda^4} \right) \cdot \frac{\Gamma(\alpha+1)}{\Gamma(t+\alpha+1)} \cdot \frac{1}{s} \right]^{(q/t)} \cdot \frac{\Gamma(\alpha+q+1)}{\Gamma(\alpha+1)}. \quad (17)$$

Equation (17) is used to retrieve IWC based on adjusted KAZR reflectivity in this study. Similarly, it also shows that the retrieved IWC is a function of N_t , Z_e , the α value of the PSD, and DDA parameterization coefficient values related to ice habits. The retrieved IWC also depends upon the parameters in the mass-dimension relationship. The mass-dimension relationship is derived from aircraft in-situ measurements during the MC3E as $M(D) = 0.00309D^{1.98}$ provided by Jingyu Wang (personal communication). Both retrieved r_e and IWC are related to the assumed α value in the PSD, N_t , ice crystal habits and radar reflectivity according to (12) and (17). Thus, in evaluating the utility of this algorithm, sensitivities to PSD, N_t , and DDA parameterization fitting coefficients related to ice crystal habits must be considered.

Sensitivity Studies

For this sensitivity study, the radar reflectivity is fixed at 7.6 dBZ, which represents the mean value of radar reflectivity along Leg 1. As shown in Fig. 10, the retrieved r_e values increase with decreasing α for a given N_t , but this relationship does not hold when $N_t > 1.0$ /Liter (L). Conversely, the retrieved r_e values increase significantly with decreasing N_t for a given α . Thus, the retrieved r_e values are negatively proportional to both α and N_t , and much more negatively proportional to N_t . The mix of particle habits

makes it difficult to confirm which kind of ice crystal habits might be occurring in sampling volume at a particular time, leading to large uncertainties in retrievals (Mace et al., 2002). Bullet rosettes and snowflakes typically yield larger values of r_e , which suggests that the retrieved r_e values with plate and column habits are less sensitive to α and N_t than r_e values retrieved with bullet rosette and snowflake habits.

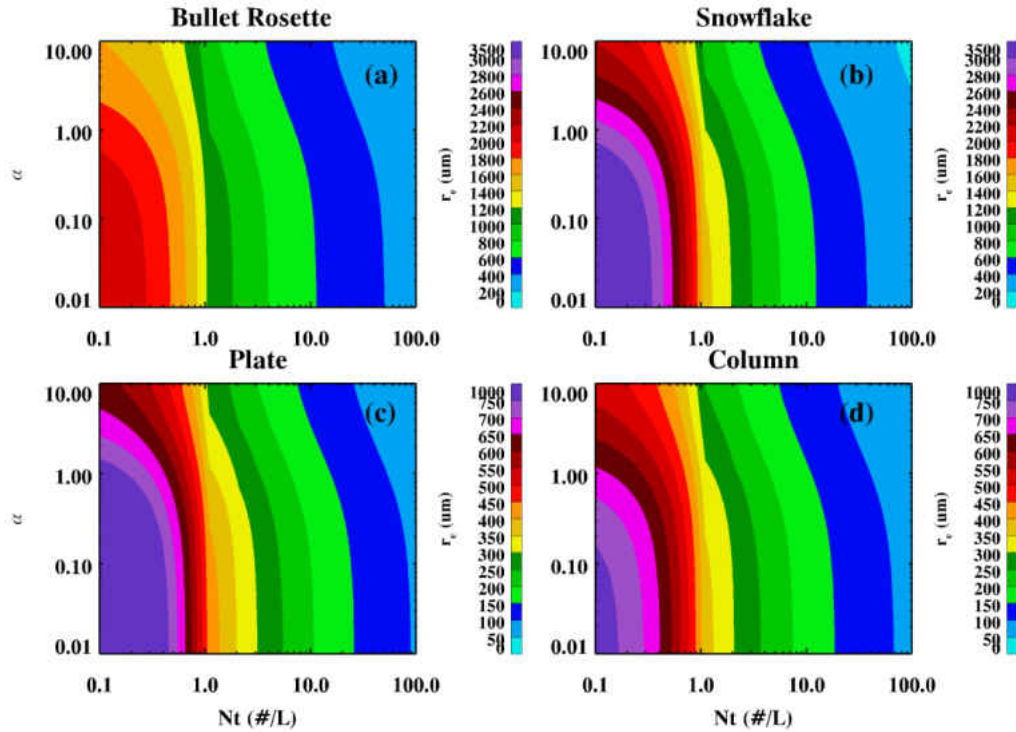


Figure 10. Dependence of radar-retrieved ice cloud effective radius r_e on N_t and α for a given ice crystal category: (a) bullet rosette, (b) snowflake, (c) plate and (d) column habits. The reflectivity value used in this sensitivity study is 7.6 dBZ, which represents the mean value of radar reflectivity along Leg 1 of the aircraft track.

In order to show more statistics results, retrieved r_e results using different α and N_t values are shown in table 4. If an α is fixed and increase or decrease 10 #/L for N_t , the retrieved r_e will decrease or increase $\sim 6.5\%$. If an N_t is fixed and increase or decrease 1 for α , the retrieved r_e will decrease or increase $\sim 6\%$.

Table.4 Retrieved r_e results at different α and N_t values

N_t (#/L)	17	27	37	47	57	67	77	87
α								
0.5	496	437	401	376	356	341	328	317
1.0	472	416	381	357	339	324	312	302
2.0	444	391	359	336	319	305	293	284
3.0	428	377	346	324	307	294	283	274

Figure 11 shows sensitivities of retrieved IWC to different α and N_t values for four kinds of ice crystal habits. The mass dimension relationship is derived from aircraft in-situ measurements during the MC3E as $M(D) = 0.00309D^{1.98}$ provided by Jingyu Wang (personal communication). As shown in Fig. 11, the dependence of the retrieved IWC are opposite to those of the retrieved r_e in Fig. 10. That is, retrieved IWC increases N_t and α . Similarly, the retrieved IWC values with plate and column habits are less sensitive to α and N_t than those with bullet rosette and snowflake habits.

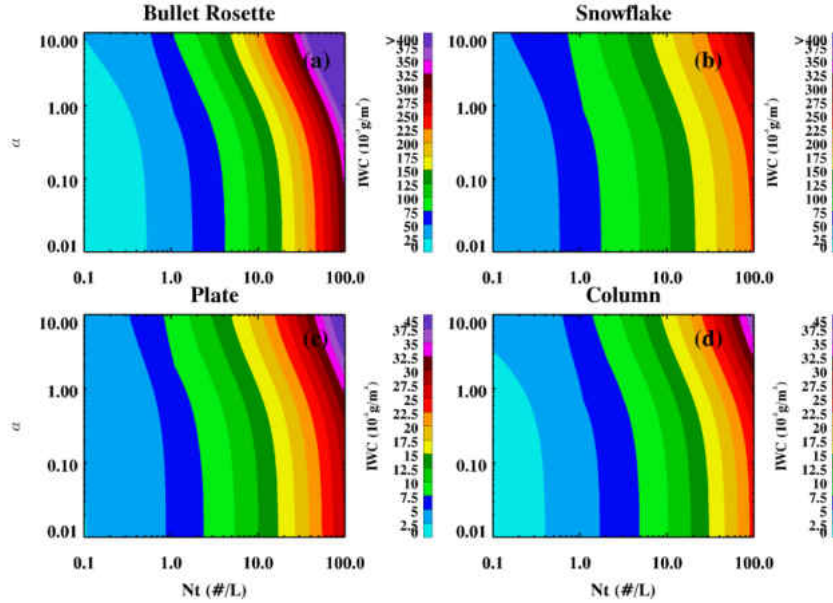


Figure 11. As in Fig. 10 but for retrieved cloud IWC .

Similarly, retrieved *IWC* results using different α and N_t values are shown in table 5. If an α is fixed and increase or decrease 10 #/L for N_t , the retrieved *IWC* will increase or decrease ~10.0%. If an N_t is fixed and increase or decrease 1 for α , the retrieved r_e will increase or decrease ~10%.

Table.5 Retrieved *IWC* results at different α and N_t values

N_t (#/L) \ α	17	27	37	47	57	67	77	87
0.5	0.167	0.206	0.238	0.266	0.29	0.312	0.333	0.352
1.0	0.185	0.228	0.263	0.294	0.321	0.346	0.368	0.39
2.0	0.209	0.259	0.299	0.333	0.364	0.392	0.418	0.442
3.0	0.226	0.279	0.322	0.359	0.392	0.422	0.45	0.476

As mentioned before, with change in temperature, the parameterized DDA fitting coefficients change slightly. However, it is still not conclusive if minor changes in DDA fitting coefficients can significantly affect retrievals. To answer this question, Fig. 12 was plotted to illustrate the retrieved ice cloud r_e and *IWC* values at different temperatures. As demonstrated in Fig. 12, with constant reflectivity, N_t and α values, the retrieved ice cloud r_e and *IWC* values are almost invariant in a range of temperatures from -20 °C to -40 °C.

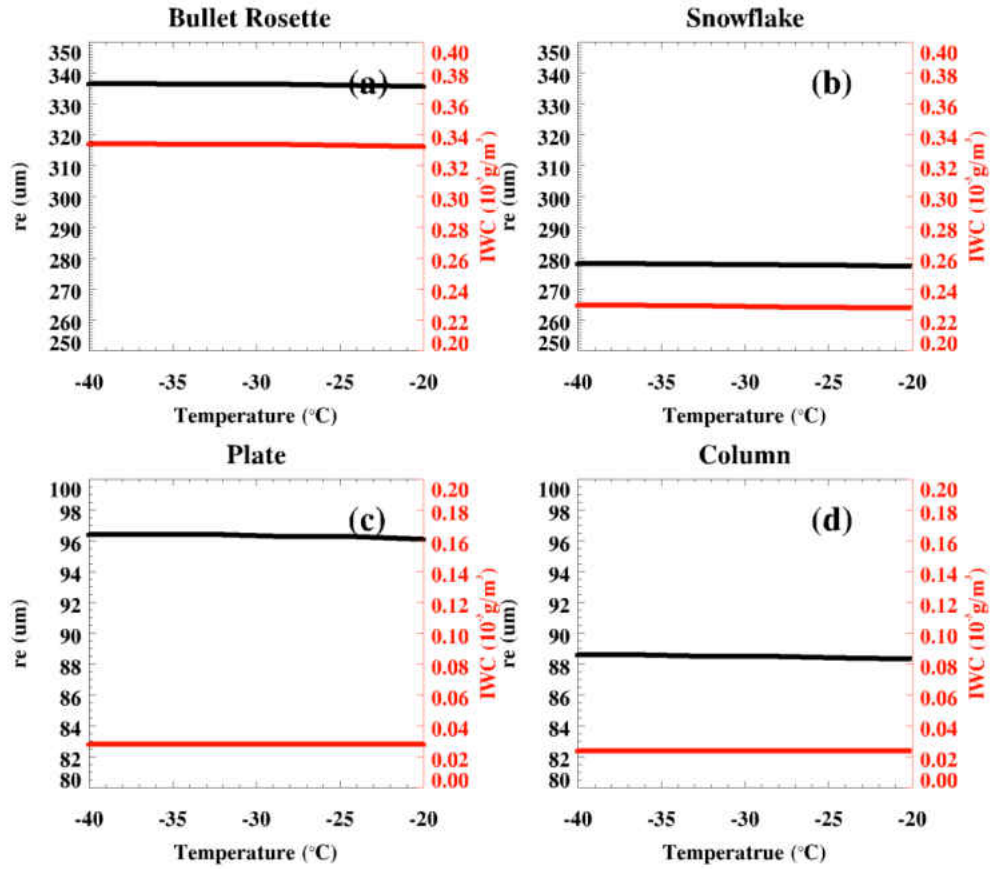


Figure 12. Dependence of radar-retrieved ice cloud r_e and IWC on temperature for a given ice crystal category: (a) bullet rosette, (b) snowflake, (c) plate and (d) column habits. The value used in this sensitivity study is $\alpha=2.0$ with 7.6 dBZ, $N_t=50 \text{ \#/L}$, which represent the mean reflectivity and N_t values along Leg 1 of the aircraft track.

Since the accuracy to which the KAZR reflectivity can be adjusted (accounting for several known radar biases) should also impact retrieval results and uncertainty, additional sensitivities for radar-retrieved r_e and IWC contingent on radar reflectivity were presented. Table 6 lists the retrieved r_e and IWC values from the radar reflectivity values of 2, 4, 6, 8 and 10 dBZ, assuming $N_t = 50 \text{ \#/L}$ and $\alpha=2.0$ for bullet rosette, snowflake, plate and column ice crystal habits. For the bullet rosette ice crystal habit, r_e

decreases $\sim 22\%$ and IWC decreases $\sim 39\%$ when the radar reflectivity drops to 2 dBZ from 6 dBZ. When the radar reflectivity increases from 6 dBZ to 10 dBZ, r_e increases $\sim 29\%$ and IWC increases $\sim 64\%$. Thus, with 2 dBZ uncertainty of KAZR reflectivity within a range from 2 to 10 dBZ, the retrieved r_e and IWC uncertainties are roughly 13% and 26%, respectively.

Table 6. Dependence of radar reflectivity-retrieved r_e and IWC on radar reflectivity with a fixed value of $N_i=50$ #/L and $\alpha=2.0$ for four ice crystal habits: bullet rosette, snowflake, plate and column

	2.0 dBZ		4.0 dBZ		6.0 dBZ		8.0 dBZ		10.0 dBZ	
	r_e (μm)	IWC (g/m^3)	r_e (μm)	IWC (g/m^3)	r_e (μm)	IWC (g/m^3)	r_e (μm)	IWC (g/m^3)	r_e (μm)	IWC (g/m^3)
Bullet rosette	232	0.17	263	0.22	298	0.28	338	0.36	383	0.46
snowflake	168	0.09	200	0.13	236	0.18	280	0.25	330	0.34
plate	62	0.012	71.6	0.017	83	0.022	97	0.03	113	0.04
column	58	0.01	66	0.014	77	0.019	89	0.025	103	0.03

CHAPTER III

RESULTS

Radar Retrievals

As discussed in the sensitivity study, the assumption of ice particle habit can affect radar retrievals. Thus, it is necessary to know which class of ice particle habit should be applied for this study. The cloud particle imager (CPI) is designed to identify ice crystal habits, but the CPI was not functional during the 20 May 2011 event. Fortunately, in-situ CPI images are available on 23 May 2011, which involved strongly forced DCS events following 20 the May 2011 storm, and it was found that most of the ice particles are aggregates of individual crystals in a range of temperatures from -30°C to -22°C (Fig. 13). Heymsfield et al. (2002a) also found that aggregates are one of the possible ice crystal habits in the stratiform region of DCSs. Therefore, the ice crystal aggregate habit was used in retrieving the DCS ice microphysical properties in this study.

The σ - D relationship is primarily a function of ice particle habit. However, the exact combination of ice crystals cannot necessarily be determined using routinely available ground-based data. The choice of σ - D relationship is usually not clear even for a single layer cirrus cloud (Mace et al., 2002). There are multiple definitions of ice crystal habits found in different studies. In this study, a bullet rosette is depicted as an aggregation of columns connected at the center (Liu, 2008) and essentially belongs to the polycrystalline habit group (Bailey and Hallett, 2004; Hong, 2007). Thus, the bullet

rosette σ - D parameterization in Fig. 6 has been used to estimate the aggregate σ - D relationship in this study.

In addition, empirical relationships (such as the aggregates σ - D relationship) developed or updated by other studies, can be easily used in the retrieval algorithm developed in this study. However, aggregates have different forms, which are complex in their composition. It is very challenging to develop a database describing the backscattering characteristics of aggregates and to confirm which kind of aggregate parameterization relationship can be used in retrieval algorithms. This is also one of the reasons that bullet rosettes σ - D relationship was used instead to perform microphysical property retrievals here.

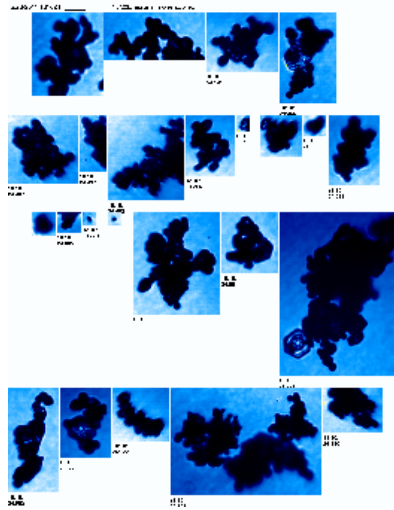


Figure 13. Cloud Particle Imaging (CPI) probe images from the 23 May 2011 MC3E event.

Figure 14 shows retrieved r_e and IWC profiles (≥ 7 km) using the ARM SGP adjusted KAZR reflectivity with a modified gamma size distribution, $\alpha=2.0$, and the bullet rosette σ - D relationship. N_t is roughly estimated by a linear relationship [N_t ($\#/cm^3$) = $height$ (km) * $0.014-0.054$], which is curve fitted from the aircraft in-situ measurements

along the aircraft track (above 4 km melting layer) as shown in Fig. 2 and 3. IWC is retrieved using (17) based upon the aircraft derived $M(D) = 0.00309D^{1.98}$ mass dimension relationship. As illustrated in Fig. 14a, the adjusted KAZR reflectivity profiles (≥ 7 km) during 20 May have significant variability both temporally and vertically. It is clear that the adjusted KAZR reflectivities before 12:00 UTC are much larger than those after that time, primarily due to the fact that the convective cores of the DCS moved over the SGP site before 12:00 UTC, and the KAZR reflectivities were associated with the SR and AC regions after 12:00 UTC. Before 12:00 UTC the adjusted KAZR reflectivities are around 20-30 dBZ at 7 km, and drop to \sim -20 dBZ above 12 km. After 12:00 UTC, KAZR reflectivities are consistently much lower, about 5-10 dBZ at 7 km and -30 dBZ at 10-11 km.

As demonstrated in Fig. 14, the temporal and vertical variations of retrieved r_e and IWC generally follow the variations of KAZR reflectivity. Both r_e and IWC retrievals before 12:00 UTC are much larger than those after 12:00 UTC, and for some periods, the retrieved r_e values are larger than 1000 μm and IWC values are higher than 3 g m^{-3} (between 7-9 km). During the aircraft flight period (13:05:39 - 17:02:04 UTC) the retrieved r_e and IWC values have no significant change temporally, but clearly have stratified r_e and IWC values vertically. The retrieved r_e values decrease from \sim 400 μm at 7 km to 50-75 μm at 11 km, and the IWC values range from \sim 0.9 g m^{-3} at 7 km to 0.01 g m^{-3} at 11 km. Similar to a previous study (Yost et al., 2010), mean r_e and IWC are shown to decrease with altitude in the top few kilometers of the cloud.

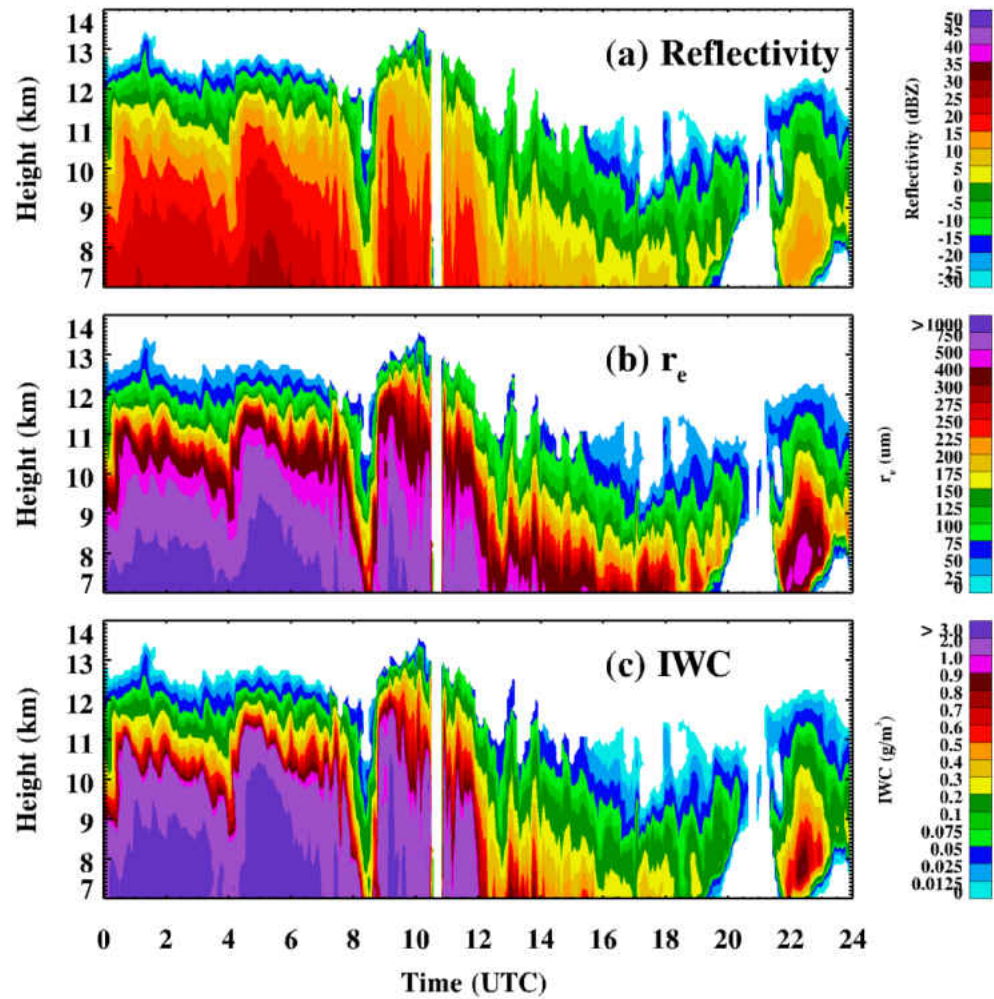


Figure 14. (a) ARM SGP adjusted KAZR reflectivity, radar-retrieved (b) r_e and (c) IWC , with modified gamma size distribution and $\alpha=2.0$ using bullet rosette σ - D relationship.

Validation with Aircraft In-situ Measurements

By using the retrieval algorithm developed in this study, the vertical profile of retrieved r_e and IWC are shown in Fig. 14. However, do these results match the aircraft

in-situ measurements? To answer this question, the aircraft in-situ measurements on 20 May are used to validate the ARM radar retrievals.

The ARM SGP KAZR has a field of view of approximately 0.2 degrees. The range resolution is around 30 meters and a sample volume of approximately $70,000 \text{ m}^3$ at a height of 8 km for the vertical radar beam. The sample volume rate of 2DC and HVPS are about 0.3 and $1.2 \text{ m}^3 \text{ s}^{-1}$ with 100 m s^{-1} airspeed. The KAZR sampling rate is on the order of 10 seconds, thus the radar sampling volume is about 4 orders of magnitude larger than those of the in situ probes. Some form of averaging is necessary in order to correctly compare the radar retrievals and aircraft in-situ measurements. In this study, the radar-retrieved r_e and IWC values in Fig. 15 are averaged into 1 min means, and then these 1 min means are compared with corresponding aircraft derived r_e and IWC values (also 1 min means) at the same altitudes ($\sim 7.6 \text{ km}$). That is, the 1 min radar retrievals have been selected when they are collocated with the aircraft measurements at the same altitudes during the two legs.

As illustrated in Fig. 15a, the adjusted radar reflectivities at the aircraft flight height ($\sim 7.6 \text{ km}$) during Leg 1 vary from 3 to 10 dBZ. As demonstrated in Fig. 15b and 15c, and summarized in Table 7, the radar retrieved r_e and IWC values during Leg 1 have excellent agreement with the aircraft in-situ measurements where most of the aircraft 1 min mean values fall within an uncertainty of 2 dBZ. The averages of radar retrieved and aircraft measured r_e during Leg 1 are $338 \text{ }\mu\text{m}$ and $337 \text{ }\mu\text{m}$, indicating 0.3% difference. Their corresponding IWC averages are 0.34 g m^{-3} , which result in no difference at all. Given the excellent agreement in both IWC and r_e between the radar retrievals and aircraft in-situ measurements during Leg 1, the adjusted KAZR reflectivity performed better than

expected despite having an apparent negative bias of 3 dB as compared to the gridded regional NEXRAD (Fig. 5c). It is well known that operational NEXRAD datasets may be less useful at higher altitudes due to lower sensitivity to smaller ice crystals. Similarly, NEXRAD calibration for system and other factors cannot be guaranteed to better than 1-2 dB using methods relying on intrinsic properties of precipitation such that this operational reference may also have been overestimating reflectivity factor during this campaign (e.g., Ryzhkov et al., 2005; Giangrande and Ryzhkov, 2005). Nevertheless, Leg 1 situations are typically better-suited for this corrected KAZR retrieval approach than Leg 2, since these times may more directly benefit from collocated UAZR profiling system measurements.

The comparisons of r_e and IWC during Leg 2 are not as promising as those from Leg 1. For Leg 2, the averages of radar-retrieved r_e and IWC are 250 μm and 0.18 g m^{-3} , and for aircraft measurements they are 305 μm and 0.23 g m^{-3} . That is, the radar retrievals are 55 μm (18%) less than r_e from aircraft in-situ measurements, and 0.05 g m^{-3} (22%) lower than IWC from aircraft in-situ measurements over the AC region of the DCS. Again as shown in Fig. 5c, the apparent biases in the adjusted KAZR reflectivity during Leg 1 and Leg 2 are -3 dB and -5 dB, respectively. Although NEXRAD observations are not well-suited to sample extended anvil regions, one may note some additional discrepancy between adjusted KAZR observations and those from the NEXRAD (~ 2 dB). In Leg 2 anvil regions, the adjusted KAZR profiles benefit less from direct comparisons with the unattenuated UAZR and surface disdrometer. Under these circumstances, the complementary platforms only act in an indirect role to provide reference to KAZR system offsets. Along these KAZR profiles, additional adjustments are made for gaseous attenuation (water vapor and oxygen), drawing from available sounding data during the

MC3E campaign (e.g., Kollias et al., 2014). However, possible in-cloud attenuation and poorly-matched sounding data may introduce additional discrepancies in the anvil regions. Notice that both the adjusted KAZR and NEXRAD reflectivities are nearly the same (~ 5 -10 dBZ) during both Legs 1 and 2, thus it is reasonable to believe that the uncertainty of the adjusted KAZR reflectivity during Leg 2 is around 2 dB. As mentioned before, an uncertainty of 2 dB can lead to a 13% difference in r_e and 26% in IWC retrievals. If 2 dB were added to the adjusted KAZR reflectivity in Leg 2, then the retrieved r_e and IWC would be 283 μm and 0.23 g m^{-3} . The differences between retrievals and in situ measurements would be reduced to -22 μm (7%) in r_e and almost no difference in IWC .

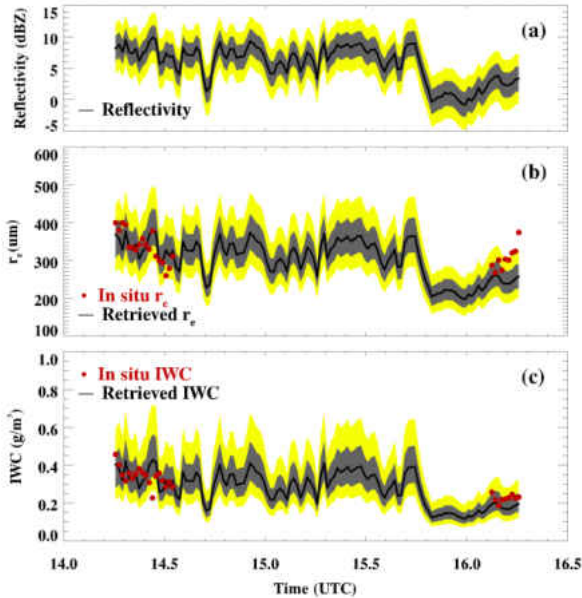


Figure 15. The 1-min averages of (a) ARM SGP adjusted KAZR reflectivity, (b) radar-retrieved r_e (black lines) and (c) IWC (black lines) with corresponding aircraft derived r_e and IWC values (filled red circles) from 2DC and HVPS measurements at the same altitudes (~ 7.6 km) as radar retrievals. The grey shaded area represents (a) 2 dB uncertainties of the adjusted KAZR reflectivity and the range of the retrieved (b) r_e and (c) IWC with 2 dB uncertainties. The yellow shaded area represents (a) 4 dB uncertainties of the adjusted KAZR reflectivity and the range of the retrieved (b) r_e and (c) IWC with 4 dB uncertainties.

Table 7. Comparison of ice cloud microphysical properties derived from aircraft measurements and retrieved from adjusted KAZR reflectivity

	Reflectivity, mean, dBZ	N_t Mean,#/L	In situ r_e mean, μm	Retrieved r_e mean, μm	Retrieved r_e SDV, μm	In situ IWC mean, g m^{-3}	Retrieved IWC mean, g m^{-3}	Retrieved IWC SDV, g m^{-3}
Leg1	7.6	47	337	338	27.5	0.34	0.34	0.055
Leg2	2.96	47	305	250	9.7	0.23	0.18	0.014

One of other possible reasons is needed to be discussed here. The modified gamma distribution with $\alpha=2$ is used in the radar retrievals, while an α of 1.5 or 1.0 may better reflect the “true” PSD over the anvil region as shown in Fig. 3. As previously discussed, the retrieved r_e and IWC will increase 3% and 6%, respectively, if $\alpha=1.5$ is used in the retrieval instead of $\alpha=2$.

Certainly, some uncertainties are present when performing this retrieval, although the retrieval results are consistent with aircraft in-situ measurements in the leg 1 SR region. First, a mean N_t value of 47 L^{-1} is assumed when generating Fig.15. However, the standard derivation of N_t is $\sim 14 \text{ L}^{-1}$, with a minimum value of 17 L^{-1} and maximum value of 86 L^{-1} during leg 1. Also, the α value varies in DCS ice clouds. $\alpha=2.0$ can be used to reproduce PSD in DCS SR regions, while $\alpha=1.0$ or 1.5 can be used to better reflect PSD in DCS AC regions. As mentioned before, if one changes N_t in $20\#/L$, it will result in 13% change in retrieved r_e values and 20% change retrieved IWC values. If one increases or decreases α by 1, it will result in 6% change in retrieved r_e values and 10% change in retrieved IWC values. In addition, an uncertainty of 2 dB can lead to a 13% difference in r_e and 26% in IWC retrievals. Thus, the total uncertainty in this retrieval is roughly estimated as 19.3% [$\text{SQRT}((13\%)^2+(6\%)^2+(13\%)^2)$] in r_e and 34.3% [$\text{SQRT}((20\%)^2+(10\%)^2+(26\%)^2)$] in IWC . Secondly, horizontal gradients in wind

velocity, wind shear, and dispersion of ice particle fall speeds may result in the aircraft and KAZR sampling different parts of clouds (Dong et al., 1998 and 2002; Heymsfield et al., 2002a). Thirdly, since there is a difference of four orders of magnitude in sampling volume between the in situ probes and the radar, the mismatched sampling volumes between the two platforms could play an important role in discrepancies (Mace et al., 2002). And, finally, uncertainties associated with using a bullet rosette σ -D relationship instead of that of aggregates cannot be ignored.

The N_t value that was used is 47 L^{-1} , which is the mean value measured using the aircraft. As there exists variation in the N_t values, the retrieved microphysical properties using in-situ measured time-series N_t values are also shown in Fig.16. The retrieval difference by using the mean N_t value and time-series N_t values are not very large (also in Table 8). However, Fig. 16 shows larger variation in microphysical properties retrieval if using time-series N_t values instead of the mean N_t value. The error at each time were also computed using the mean N_t value to do the retrieval, and the mean absolute error are $1.9 \mu\text{m}$ for r_e and 0.006 g m^{-3} for IWC in leg1, and $56.2 \mu\text{m}$ for r_e and 0.04 g m^{-3} for IWC in leg2. Using the time-series N_t value to do the retrieval instead, the mean absolute error are $10.5 \mu\text{m}$ for r_e and 0.0035 g m^{-3} for IWC in leg1, and $54.6 \mu\text{m}$ for r_e and 0.04 g m^{-3} for IWC in leg2.

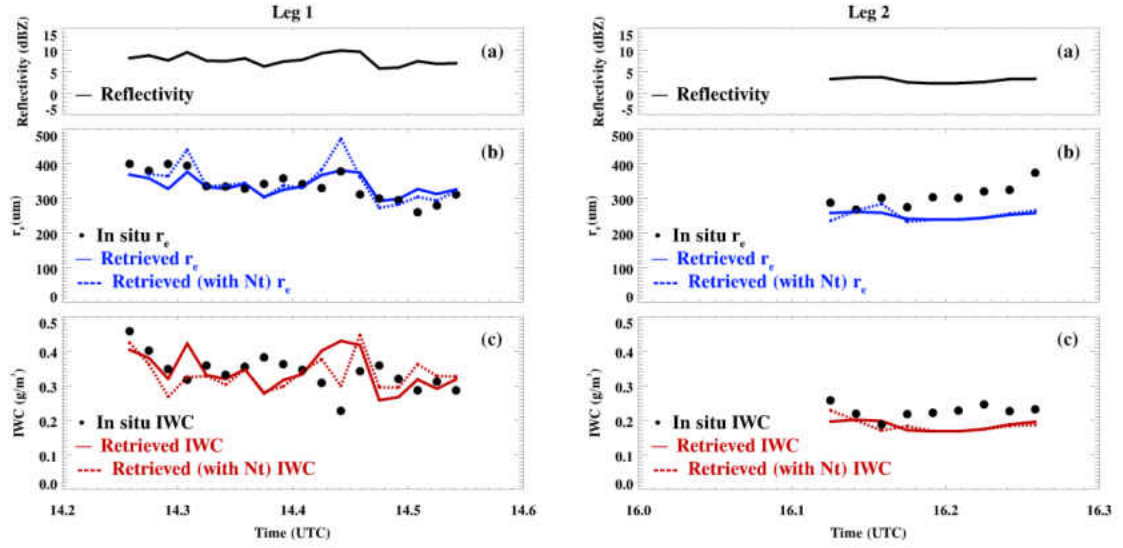


Figure 16. Comparisons between the retrieved (b) r_e and (c) IWC using the mean N_t value of 47 L^{-1} (solid lines) and in-situ measured time-series N_t values (dashed lines) using (a) 1-min averaged adjusted KAZR reflectivity.

Table 8. Comparison of ice cloud microphysical properties derived from aircraft measurements and retrieved from adjusted KAZR reflectivity using the mean N_t value and in-situ time-series N_t values.

	Reflectivity, mean, dBZ	N_t Mean, #/L	In situ r_e mean, μm	Retrieved r_e mean, μm	Retrieved r_e SDV, μm	In situ IWC mean, g m^{-3}	Retrieved IWC mean, g m^{-3}	Retrieved IWC SDV, g m^{-3}
Leg1	7.6	47	337	338	27.5	0.34	0.34	0.055
Leg2	2.96	47	305	250	9.7	0.23	0.18	0.014
Leg1	7.6	47	337	344	52.8	0.34	0.33	0.047
Leg2	2.96	47	305	251	17.5	0.23	0.18	0.019

Validation of the Assumptions in the Radar-based Retrieval Algorithms

The relationship between the reflectivity, PSD and the ice habits is shown in (7). In this section, calculated reflectivity using aircraft measurements will be provided to further prove that the assumptions used in the retrieval algorithm are reasonable. The aircraft in-situ measured PSD will be used as $N(D)$ in (7), and DDA results for 11 kinds

of ice habits will be used to provide the σ information in (7). Figure 17 compares the calculated reflectivity using 11 kinds of ice habits, σ information from DDA, and aircraft measured PSD with adjusted KAZR reflectivity in Leg 1 and 2. The calculated reflectivity using bullet rosette backscattering information from DDA is close to the adjusted KAZR reflectivity, especially in Leg 1. For Leg 2, the calculated reflectivity using dendrite snowflake backscattering information from DDA is closer to the adjusted KAZR reflectivity. This may also explain discrepancies with the retrievals during Leg 2. More importantly, the consistency between adjusted KAZR reflectivity and calculated reflectivity further indicates that the assumptions (modified gamma PSD assumption and bullet rosette σ -D parameterized relationship) used in the radar retrieval algorithm are reasonable.

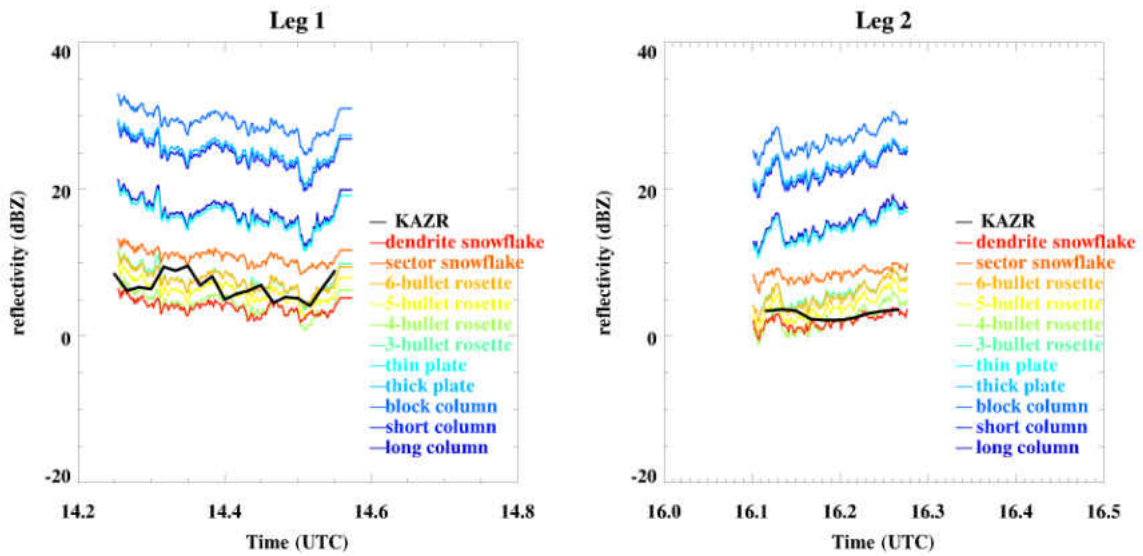


Figure 17. Comparisons between the aircraft calculated using 11 kinds of ice habits σ information (same as Fig. 6) from DDA and aircraft measured PSD and the adjusted KAZR reflectivity (black line) in (a) Leg 1 and (b) Leg 2.

Comparisons with GOES Satellite Retrievals

As mentioned above, GOES retrieved DCS CTH and particle size have not yet been fully validated. Thus, in this section, the GOES-satellite-retrieved DCS ice cloud CTH and particle size will be compared with the ARM KAZR measurements and retrievals during the MC3E.

Cloud Top Height (CTH)

Since there are significant spatial and temporal differences between the ground-based remote sensors and satellite observations, such as the relatively small sizes of the ARM KAZR field of view as compared to the much larger satellite field of view, temporal and spatial scales should be matched as closely as possible during the surface-satellite comparison. Based on the results and discussions in Dong et al. (2002, 2008), 100 km averaging yields the best match between temporally averaged surface results and spatially averaged satellite results assuming that the 1 h averaging interval is equivalent to a frozen turbulence spatial scale of 108 km with high-level winds of 30 m s⁻¹. Figure 18 shows the ARM-adjusted KAZR reflectivity with GOES retrieved CTH during MC3E. On average, GOES CTHs agree with the ARM CTHs within 0.5 km. For all cases, over the anvil regions, the GOES derived CTHs agree well with the ARM CTHs. However, near convective cores with heavy precipitation, the GOES derived CTHs are 1-2 km higher than the radar CTHs possibly because radar signals are attenuated by the heavy precipitation. For all of the DCS cases during MC3E, the GOES retrieved CTHs are on average about 0.2 km higher than the ARM CTHs with relatively large differences for individual events due to the attenuation of radar signals with heavy precipitation and large liquid paths. Figure 19 shows the corresponding scatterplots of the

GOES and ARM retrieved CTHs with the mean values, mean standard deviations, correlation coefficients, and root mean square errors (RMSE). These statistical results reveal that the GOES CTHs agree with the ARM observations very well with small mean difference, standard deviation, and RMSE.

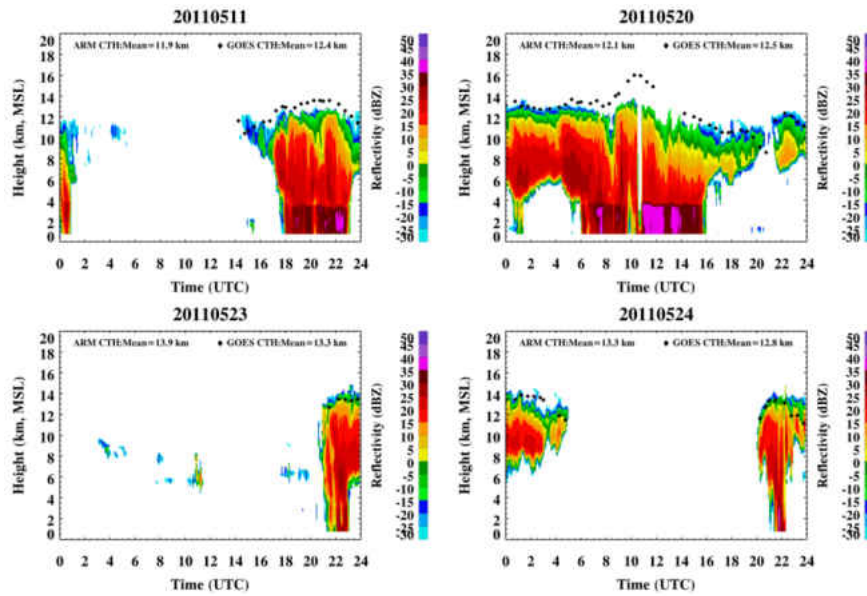


Figure 18. The DOE ARM KAZR derived CTHs (1-hour average) and matched GOES derived CTHs ($1^{\circ} \times 1^{\circ}$ grid box, diamonds) for the DCSs over the ARM SGP site during the MC3E.

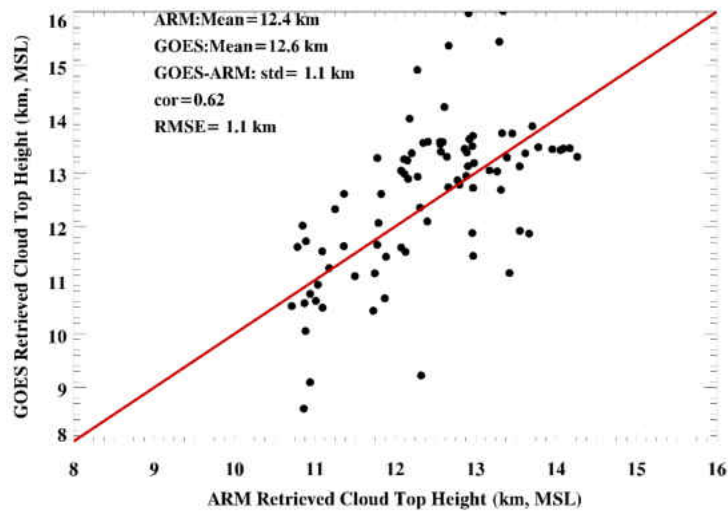


Figure 19. As in Fig. 18, except scatterplots for all four cases during MC3E.

DCS Ice Cloud Particle Size

It is well known that ice particles have a variety of shapes that are highly irregular and non-spherical (Yang et al., 2003). Therefore, it is common to classify ice crystals by their length or maximum dimension D , their width W , and the size distribution $n(D)$. To be consistent with the VISST cloud retrieval algorithms, the equation used to retrieve effective diameter D_e from the ARM KAZR reflectivity is modified as to (Minnis et al., 1998; Yost et al., 2010)

$$D_e = \frac{\int DW^2n(D)dD}{\int WDn(D)dD}. \quad (20)$$

In this study, (20) is used for both ARM and GOES D_e retrievals. Two ice crystal habits are used in the ARM retrievals: hexagonal columns and bullet rosettes. Wyser and Yang (1998) determined a functional relationship between L and D for the case of hexagonal columns given by $D=2.5 L^{0.6}$. For the bullet rosettes ice habit, the aspect ratio (D/L) is assumed to be 0.4 ($D=0.4 L$). This aspect ratio of bullets rosettes was developed using aircraft CPI measurements (Heymsfield et al., 2003).

Figure 20 shows the retrieved D_e values assuming hexagonal column and bullet rosette ice habits from the adjusted KAZR reflectivity, and only daytime results are used to compare with the GOES retrievals in this study. As demonstrated in Fig. 20, the KAZR retrieved D_e values with hexagonal column habits are much lower than those with bullet rosette habits. In addition, the KAZR retrieved D_e values with hexagonal column habits also much lower than those (60 μm) from the single-layered cirrus clouds at the SGP site (Table 1, Mace et al., 2005). Therefore, it is concluded that the KAZR retrieved D_e values using hexagonal columns habits are too small to be trusted in this study. To future

investigate which kind of habits should be used in ARM retrievals, Fig. 21 shows the CPI images collected on 23 May 2011 at temperatures around -40°C . Compared to Fig. 13, more small ice particles were collected by CPI shown in Fig. 21 indicating that D_e decreases with altitude in the upper layer of deep convective clouds (Yost et al., 2010). Figure 21 also shows that almost all large ice particles imaged by CPI are aggregated. In addition, as mentioned in the Radar Retrievals section, the bullet rosettes and aggregates have most similar backscatter information for cloud radar. Therefore, it is reasonable to assume bullet rosettes for retrieving the DCS ice cloud microphysical properties in this study.

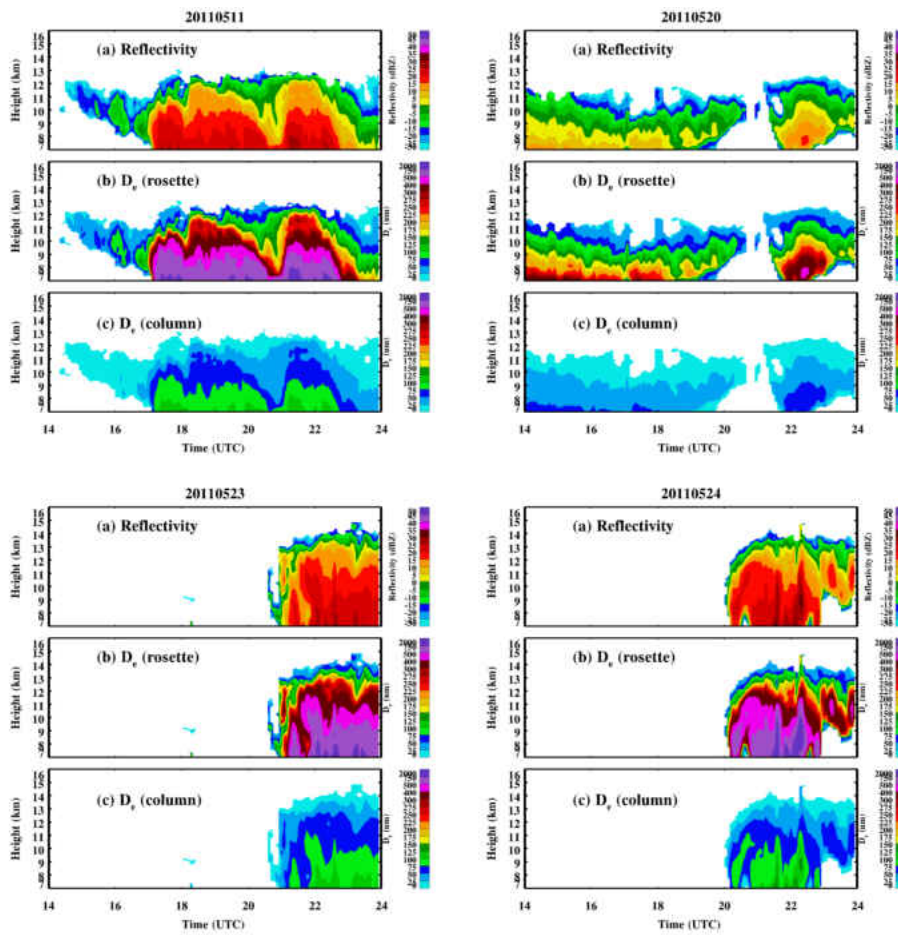


Figure 20. (a) ARM SGP adjusted KAZR reflectivity, (b) radar-retrieved D_e assuming hexagonal columns habits and (c) D_e assuming bullet rosette habits.

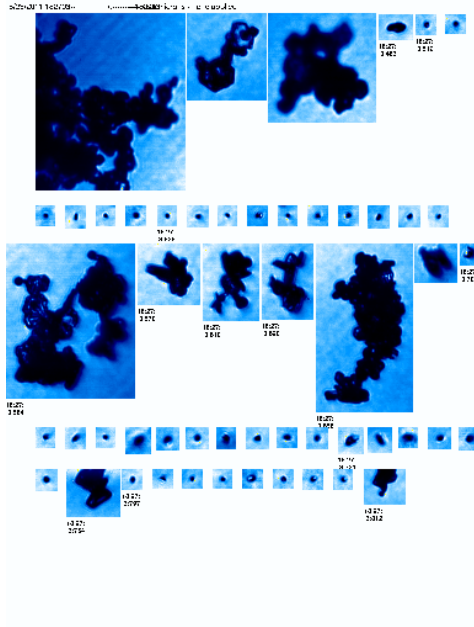


Figure 21. As in Fig. 13, except for at temperatures around -40°C .

Above, as discussed, the bullet rosette ice habits can be used in the ARM retrievals. Now, another question need to be answer: if both KAZR and GOES retrieved D_e values are correct, are they the same?

The speed of a cloud system at 10 km with respect to the ground, on average, is about $25\text{-}30\text{ m s}^{-1}$ from the ARM merged sounding profiles for the DCS cases during the MC3E. Following the spatial and temporal averaging method in *Dong et al. (2002 and 2008)*, GOES retrievals are averaged within a $1^{\circ}\times 1^{\circ}$ grid box centered over the ARM SGP site, while ARM retrievals are averaged within 1 hr (± 0.5 hr GOES image). According to *Minnis et al. (2008)*, the satellite retrieved H_{eff} should represent an optical depth of ~ 1 down from the cloud top, which corresponds to $\sim 1\text{-}2$ km in ice clouds, even for optically thick ice clouds. Following this method, a KAZR reflectivity threshold (-5 dBZ/ -2.5 dBZ/ 0 dBZ/ 2.5 dBZ) was set up instead of the optical depth. Then average the KAZR retrieved D_e values from cloud top to the altitudes where the KAZR reflectivity

threshold at to calculate the layer mean D_e values, and finally use these layer-mean D_e values to compare with GOES retrievals.

Figure 22 shows the dependence upon different reflectivity thresholds (-5 dBZ/ -2.5 dBZ/ 0 dBZ/ 2.5 dBZ). Mean, mean difference, RMSE and correlation coefficient values between KAZR and GOES retrieved D_e are calculated and shown in Table 9. The definition of total difference is

$$\text{Total difference} = \sum_1^{\text{sample}} \left| \frac{De_{KAZR} - De_{GOES}}{De_{GOES}} \right|, \quad (21)$$

where De_{KAZR} and De_{GOES} represent the KAZR and GOES retrieved D_e , respectively. Though the 0 dBZ has the lowest RMSE and mean difference, not the highest Correlation coefficient. However, if the 2 dB uncertainties from adjusted KAZR reflectivity was considered, the selection for 0 dBZ may be a very reasonable choice. This means that the satellite retrieved D_e can be compared to the ARM KAZR retrieved D_e values averaged from cloud top down to where the reflectivity is 0 dBZ.

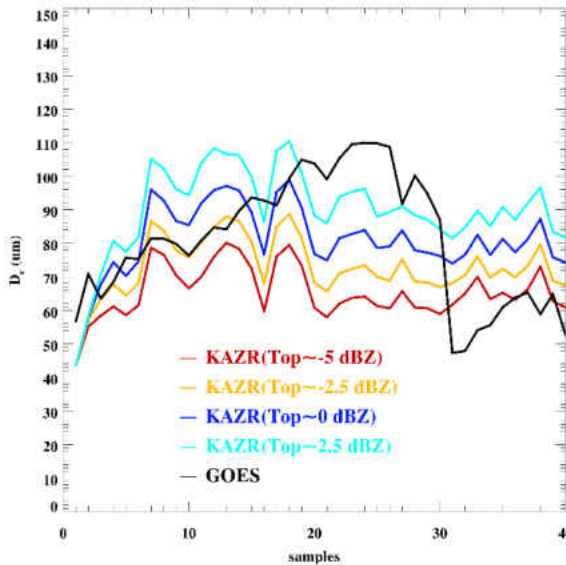


Figure 22. GOES and ARM retrieved D_e averaged at different reflectivity thresholds. The mean value of GOES retrieved D_e is 81 um.

Table 9. Mean, mean difference, RMSE, and correlation coefficient values of ARM and GOES retrieved D_e .

	-5 dBZ	-2.5 dBZ	0 dBZ	2.5 dBZ
Mean (μm)	65.6	72.9	81	90
Mean(KAZR)-Mean(GOES) (μm)	-15.4	-8.1	0	9
Total difference (μm)	9	7.8	8.4	10
RMSE	24.6	20.3	18	20
Correlation coefficient	0.15	0.26	0.36	0.42

Comparisons between GOES retrievals and KAZR layer-mean using 0 dBZ as a reflectivity threshold are shown in Fig. 23. The KAZR-retrieved D_e values with hexagonal column habits are much lower than GOES retrievals, while those with bullet rosette habits are very close to GOES retrievals. As illustrated in Fig. 23, the averaged KAZR D_e values for the four selected cases are around 81 μm (for bullet rosettes), while the GOES retrievals range from 51.2 μm on 23 May to 101.1 μm on 20 May.

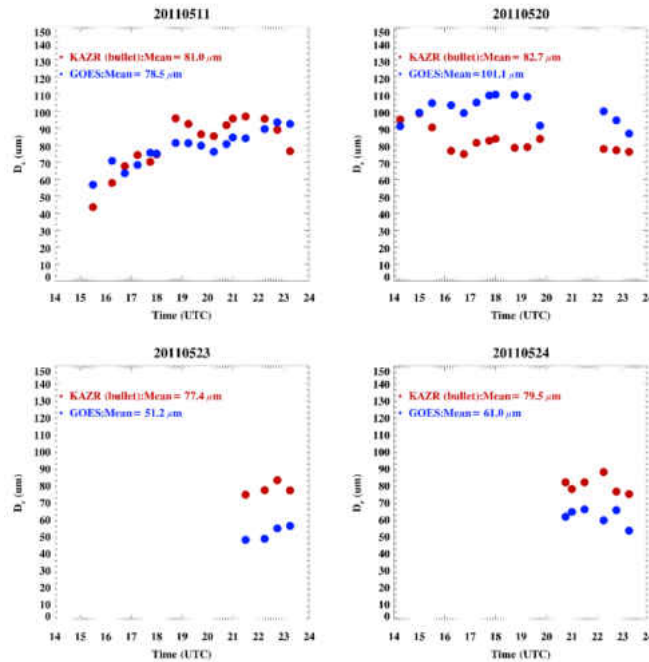


Figure 23. Comparisons between KAZR-retrieved (with bullet rosettes ice habits) and GOES retrieved D_e values during the MC3E.

In order to explain the physical meaning of the reflectivity threshold, a comparison between the height of the 0 dBZ isosurface and H_{eff} is shown in Fig. 24. On average, the height of the 0 dBZ isosurface is about 0.8 km lower than the GOES retrieved H_{eff} (11 km), which corresponds to the cloud radiative center. To get more solid results, more cases must be examined and analyzed statistically.

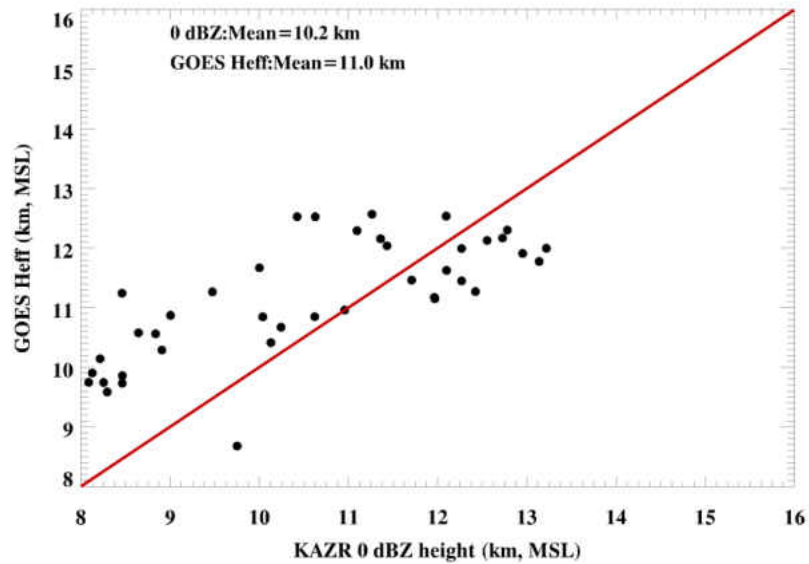


Figure 24. Comparison between the 0 dBZ height and the GOES retrieved effective cloud height H_{eff} .

CHAPTER IV

CONCLUSIONS AND FUTURE WORK

Conclusions

In this study, a new algorithm for retrieving DCS ice cloud microphysical properties has been developed using the ARM SGP adjusted KAZR reflectivity with a modified gamma size distribution, $\alpha=2.0$, a bullet rosette σ - D relationship, and data collected during the MC3E field experiment. The ARM retrievals are then compared with aircraft in situ measurements and GOES satellite retrievals collected/produced during the MC3E. The findings from this study are summarized as follows:

- 1) A new algorithm has been developed for retrieving DCS ice cloud microphysical properties using adjusted KAZR reflectivity. The PSD size parameter, $\alpha=2$, in the modified gamma distribution and the shape of the ice crystal habit (aggregate) have been determined using aircraft in situ measurements collected during the MC3E. The adjusted KAZR reflectivity, determined α value, and use of bullet rosette σ - D relationship influence the degree of success for this retrieval method.
- 2) The radar retrieved r_e and IWC basically follow the variations of KAZR reflectivity on 20 May 2011. Both r_e and IWC retrievals before 12:00 UTC are much larger than those after 12:00 UTC, and for some periods, the retrieved r_e values are larger than 1000 μm and IWC values are higher than 3 g m^{-3} at altitudes of 7-9 km. During the aircraft flight period (13:05:39-17:02:04 UTC), the

retrieved r_e and IWC values have no significant temporal change, but clearly have vertically stratified values. The retrieved r_e values decrease from $\sim 400 \mu\text{m}$ at 7 km to $50\text{-}75 \mu\text{m}$ at 11 km, and the IWC values range from $\sim 0.9 \text{ g m}^{-3}$ at 7 km to 0.01 g m^{-3} at 11 km.

- 3) The averaged IWC and r_e from KAZR retrievals over the SR region of the DCS are 0.34 g m^{-3} and $338 \mu\text{m}$, in excellent agreement with the aircraft in-situ measured IWC (0.34 g m^{-3}) and r_e ($337 \mu\text{m}$). Over the AC region, the retrieved and measured IWC s are 0.18 g m^{-3} and 0.23 g m^{-3} , and the r_e values are $250 \mu\text{m}$ and $305 \mu\text{m}$, respectively. The radar retrieved r_e and IWC can increase to $283 \mu\text{m}$ and 0.23 g m^{-3} if 2 dB of uncertainty is added to the adjusted KAZR reflectivity over the AC region, with sensitivities of 13%/2 dB in r_e and 26%/2 dB in IWC .
- 4) GOES retrieved CTH, on average, is about 0.2 km higher than ARM CTH, which results from cloud radar attenuation in heavy precipitation. Bullet rosette habits should be used for retrieving DCS ice cloud microphysical properties from KAZR reflectivity. Vertically, the satellites retrieved D_e can be compared to the ARM KAZR retrieved D_e values averaged from cloud top down to where the reflectivity is 0 dBZ.

Future Work

Apply Retrieval Method to NEXRAD Radar Reflectivity

Since NEXRAD radar reflectivity has little attenuation during the DCS events, it is useful to apply the KAZR-based retrieval algorithm to NEXRAD data. As shown in Fig. 5, the reflectivity differences between adjusted KAZR and NEXRAD are -4 dB on

average in the DCS ice cloud, which is in a reasonable difference range. The same modified gamma PSD and N_t values are still used here, as they are not affected by the change of radar wavelength used in the algorithm. However, the s and t values from DDA should be parameterized for the NEXRAD wavelength (10 cm). Also, the wavelength value used in (12) should be changed to 10 cm. Figure 25 shows the 11 non-spherical σ values (at 10 cm, -25 °C) (colored lines) and four regrouped ice crystal habits (symbols) as a function of D .

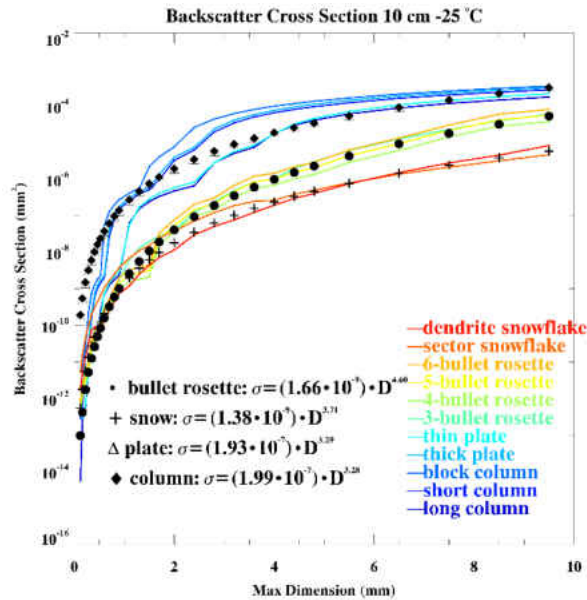


Figure 25. As in Fig. 6 except for 10 cm wavelength and -25 °C.

With the same modified gamma PSD, N_b and new DDA parameterization coefficients, r_e and IWC can be retrieved using NEXRAD reflectivity. As illustrated in Fig. 26a, NEXRAD reflectivity factors at the aircraft flight height (~ 7.6 km) vary from 0 to 15 dBZ. As demonstrated in Figs. 26b and 26c, and summarized in Table 10, the NEXRAD radar retrieved r_e and IWC values during the two legs were higher than the aircraft in-situ measurements. However, most of the aircraft 1-min mean values fall

within uncertainty ranges associated with a reflectivity uncertainty of 4 dB. The average -4 dB reflectivity difference results in r_e values retrieved from NEXRAD reflectivity and aircraft measurements during Leg 1 of 356 μm and 337 μm —a 6% difference. Their corresponding retrieved and aircraft measured IWC averages are 0.36 g m^{-3} and 0.34 g m^{-3} , also a 6% difference. For Leg 2, the averages of radar-retrieved r_e and IWC are 304 μm and 0.27 g m^{-3} , and for aircraft measurements, they are 305 μm and 0.23 g m^{-3} , resulting in almost no difference at all for r_e and a 17% difference in IWC . These results shown as a motivation to apply the KAZR based method to NEXRAD radar reflectivity, which will include more DCS cases and provide more accurate comparisons between the NEXRAD retrievals and aircraft in-situ measurements during MC3E.

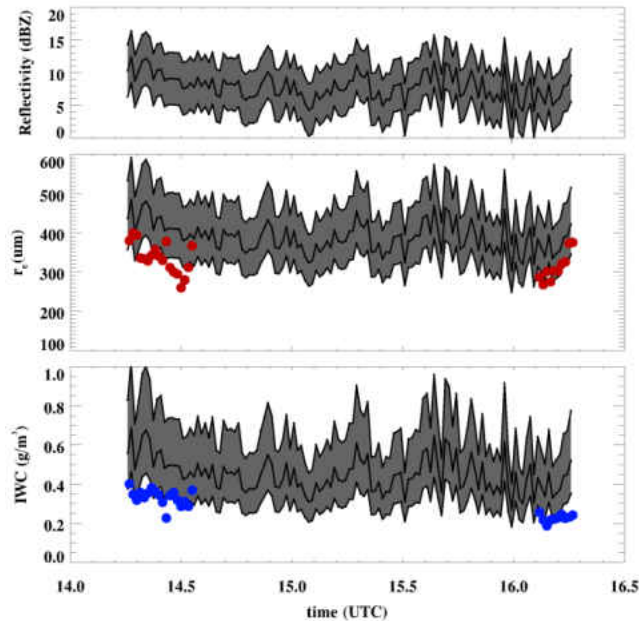


Figure 26. The 1-min averages of (a) NEXRAD reflectivity along aircraft track, (b) radar-retrieved r_e (black lines) and (c) IWC (black lines) with corresponding aircraft derived r_e (filled red circles) and IWC values (filled blue circles) from 2DC and HVPS measurements at the same altitudes (~ 7.6 km) as radar retrievals. The grey shaded area represents (a) 4 dB uncertainties of the NEXRAD reflectivity and the ranges of the retrieved (b) r_e and (c) IWC with 4 dB uncertainties.

Table 10. Comparison of ice cloud microphysical properties derived from aircraft measurements and retrieved from NEXRAD reflectivity

	Reflectivity, mean, dBZ	N_t Mean, #/cm ³	In situ r_e mean, μm	Retrieved r_e mean, μm	Retrieved r_e SDV, μm	In situ IWC mean, g/m ³	Retrieved IWC Mean, g/m ³	Retrieved IWC SDV, g/m ³
Leg1	9.8	0.047	337	426	32	0.34	0.54	0.08
Leg2	7.0	0.047	305	371	28	0.23	0.41	0.06
Leg1	13.8	0.047	337	520	39	0.34	0.80	0.12
Leg2	11.0	0.047	305	454	35	0.23	0.61	0.09
Leg1	5.8	0.047	337	356	26	0.34	0.36	0.05
Leg2	3.0	0.047	305	304	23	0.23	0.27	0.04

Improve Satellite Nighttime Particle Size Retrieval

Diurnal variations of DCS ice cloud properties are important for understanding the Earth radiation and heat budgets and for improving climate models. Thus, retrieval of a full range of cloud properties during nighttime will greatly benefit numerical weather predictions (Minnis et al., 2012). Most methods have focused on retrieving cloud properties, such as τ and D_e , during the daytime because cloud optical depth τ is retrieved from the visible channel (Minnis et al., 1995). During both day and night it is possible to estimate cloud heights, but retrievals of τ and D_e have been limited to optically thin clouds ($\tau < \sim 6$) because of the constraints of the blackbody limit (Minnis et al., 2012). Here, two steps are proposed for improving satellite-based nighttime D_e retrievals. The KAZR retrievals should be the same for both day and night. The GOES nighttime D_e retrievals are much lower than the KAZR nighttime retrievals (Fig. 27). The difference in GOES retrievals is due to GOES nighttime retrieval limitations. First, empirical relationships will be developed between daytime D_e and other cloud parameters that should be available during both day and night. Then apply this/these relationship(s) to retrieve nighttime D_e . Secondly, use the KAZR D_e retrievals as “ground-truth” to modify

the relationship(s) and implement the modified relationship to calculate nighttime D_e values.

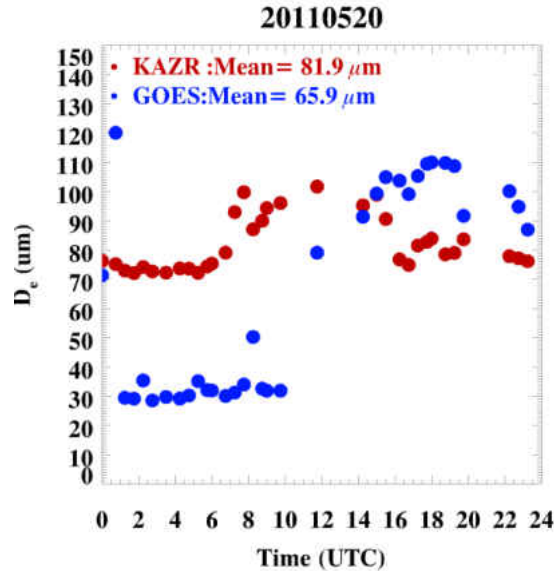


Figure 27. Comparison between KAZR-retrieved (with hexagonal column and bullet rosette ice habits) and GOES-retrieved (during both daytime and nighttime) D_e on 20 May 2011.

Development of Algorithms for Retrieving Cloud Microphysical Properties of Mixed-phase and Liquid/precipitation Layers of DCSs during MC3E

In a series of studies, this being the first, algorithms for retrieving cloud microphysical properties of the ice-phase, mixed-phase and liquid/precipitation layers of DCSs observed during MC3E will be developed. These retrievals will be validated using UND Citation II research aircraft in-situ measurements. The first step, completed herein, focuses on developing a new retrieval method for the DCS ice cloud microphysical properties and validates the retrievals using the aircraft provided best-estimate r_e , IWC and PSD. The next steps develop new algorithms for retrieving the cloud microphysical properties of the mixed-phase layer and liquid/precipitation layer of DCSs using ARM SGP adjusted KAZR reflectivity and other measurements obtained during the MC3E.

APPENDIX

Appendix

List of Acronyms and Symbols

AC	Anvil cloud
AC _{trans}	Transitional anvil
AC _{thk}	Thick Anvil
ARM	Atmospheric Radiation Measurement
CALIPSO	Cloud-Aerosol Lidar and Infrared Pathfinder Satellite Observations
CC	Convective core
CDP	Cloud Droplet Probe
CERES	Clouds and Earth's Radiant Energy System
CPI	Cloud particle imager
CRYSTAL	Cirrus Regional Study of Tropical Anvils and Cirrus Layers
CSA	Convective Startiform Anvil classification
CTH	Cloud top heights
DCS	Deep Convective Systems
DDA	Discrete Dipole Approximation
DMT	Droplet Measurement Technologies
DWR	Dual Wavelength Ratio
ECMWF	European Centre for Medium Range Weather Forecasts
FACE	Florida Area Cirrus Experiment
FDTD	Finite-difference time domain method
GOES	Geostationary Operational Environmental Satellite
HVPS	High Volume Precipitation Spectrometer
IR	Infrared
IWC	Ice water content
JWD	Joss-Waldvogel impact disdrometer
KAZR	Ka-band ARM Zenith Radar
LWP	Liquid water path
MC3E	Midlatitude Continental Convective Clouds Experiment
MWR	Microwave radiometer (MWR)
MODIS	Aqua Moderate Resolution Imaging Spectroradiometer
NEXRAD	Next Generation Weather Radar
NSAS	National Aeronautics and Space Administration
PMS	Particle Measurement System
PSD	Particle size distribution
RMSE	Root mean square errors
RUC	Rapid Update Cycle
SCATDB	Scattering database

SGP	Southern Great Plain
SI	Solar infrared
SIST	Solar-infrared Infrared Split-Window Technique
SR	Stratiform rain
SWC	Split-window channel
SZA	Solar zenith angle
TOA	Top of the atmosphere
TWC	Total water content
UAZR	UHF ARM Zenith Rada
UND	University of North Dakota
VIS	Visible
VISST	Visible Infrared Solar-infrared Split-Window Technique
2DC	Two-dimensional cloud probe
α	Size distribution shape parameter
D	Particle dimension
D_e	Effective diameter
$D_{e_{KAZR}}$	KAZR retrieved effective diameter
$D_{e_{GOES}}$	GOES retrieved effective diameter
H_{eff}	Cloud effective height
$ K_w ^2$	Dielectric factor for water
m	Complex refractive index
N_t	Total number concentration
Γ	Gamma function
s	DDA parameterization coefficient
t	DDA parameterization coefficient
p	mass-dimension coefficient
q	mass-dimension coefficient
r_e	Effective radius
σ	Backscatter cross section
T_{eff}	Cloud effective temperature
Z_e	Equivalent reflectivity factor for water droplets
Z_i	Radar reflectivity factor for ice particles

REFERENCES CITED

- Atlas, D., S. Y. Matrosov, A. J. Heymsfield, M.-D. Chou, and D. B. Wolf (1995), Radar and radiation properties of ice clouds, *J. Appl. Meteorol.*, 34, 2329–2345.
- Aydin, K., and C. Tang (1997), Relationships between IWC and polarimetric radar measurands at 94 and 220 GHz for hexagonal columns and plates, *J. Atmos. Oceanic Technol.*, 14, 1055–1063.
- Aydin, K., and T. M. Walsh (1999), Millimeter wave scattering from spatial and planar bullet rosettes, *IEEE Trans. Geosci. Remote Sens.*, 37, 1138–1150.
- Bailey, M., J. Hallett (2004), Growth Rates and Habits of Ice Crystals between -20° and -70°C . *J. Atmos. Sci.*, 61, 514–544.
- Benjamin, S. G., et al. (2004), An hourly assimilation–forecast cycle: The RUC, *Mon. Weather Rev.*, 132(2), 495–518.
- Clothiaux, E. E., T. P. Ackerman, G. G. Mace, K. P. Moran, R. T. Marchand, M. A. Miller, B. E. Martner, 2000: Objective Determination of Cloud Heights and Radar Reflectivities Using a Combination of Active Remote Sensors at the ARM CART Sites. *J. Appl. Meteor.*, 39, 645–665.
- Comstock, Jennifer M., and Coauthors, 2007: An Intercomparison of Microphysical Retrieval Algorithms for Upper-Tropospheric Ice Clouds. *Bull. Amer. Meteor. Soc.*, 88, 191–204
- Delanoë, J., and R. J. Hogan (2008), A variational scheme for retrieving ice cloud properties from combined radar, lidar, and infrared radiometer, *J. Geophys. Res.*, 113, D07204.
- Deng, M., and G. Mace (2006), Cirrus microphysical properties and air motion statistics using cloud radar Doppler moments. Part I: Algorithm description, *J. Appl. Meteorol. Climatol.*, 45, 1690–1709
- Dong, X., B.A.Wielicki, B. Xi, Y. Hu, G.G. Mace, S. Benson, F. Rose, S. Kato, T. Charlock and P. Minnis (2008), Using observations of deep convective systems to constrain atmospheric column absorption in the optically thick limit. *J. Geophys. Res.*, 113, D10206.

- Dong X., P. Minnis, G.G. Mace, W.L. Smith Jr, M. Poellt, R. Marchand, and Anita D. Rapp, 2002: Comparison of stratus cloud properties deduced from surface, GOES, and aircraft data during the March 2000 ARM Cloud IOP. *J. Atmos. Sci.*, 59, 3265-3284.
- Dong X., T.P. Ackerman, and E.E. Clothiaux, 1998: Parameterizations of Microphysical and Radiative Properties of Boundary Layer Stratus from Ground-based measurements. *J. Geophys. Res.*, 102, 31,681-31,393.
- Donovan, D. P., and A. C. A. P. Van Lammeren (2001), Cloud effective particle size and water content profile retrievals using combined lidar and radar observations: 1. Theory and examples, *J. Geophys. Res.*, 106, 27,425–27,448.
- Donovan, D. P., M. Quante, I. Schlimme, and A. Macke (2004), Use of equivalent spheres to model the relation between radar reflectivity and optical extinction of ice cloud particles, *Appl. Opt.*, 43, 4929–4940.
- Draine, B. T., and P. J. Flatau (1994), Discrete-dipole approximation for scattering calculations, *J. Opt. Soc. Am. A*, 11, 1491–1499.
- Feng, Z., S. McFarlane, C. Schumacher, S. Ellis, J. Comstock, and N. Bharadwaj (2014): Constructing A Merged Cloud-Precipitation Radar Dataset for Tropical Convective Clouds during the DYNAMO/AMIE Experiment at Addu Atoll. *J. Atmos. Oceanic Technol.*, 31, 1021-1024.
- Feng, Z., X. Dong, B. Xi (2009), A Method to Merge WSR-88D Data with ARM SGP Millimeter Cloud Radar Data by Studying Deep Convective Systems. *J. Atmos. Oceanic Technol.*, 26, 958–971.
- Feng, Z., X. Dong, B. Xi, C. Schumacher, P. Minnis, and M. Khaiyer (2011), Top-of-atmosphere radiation budget of convective core/stratiform rain and anvil clouds from deep convective systems, *J. Geophys. Res.*, 116, D23202.
- Feng, Z., X. Dong, B. Xi, S. A. McFarlane, A. Kennedy, B. Lin, and P. Minnis (2012), Life cycle of midlatitude deep convective systems in a Lagrangian framework, *J. Geophys. Res.*, 117, D23201.
- Fu, Q. (1996), An accurate parameterization of the solar radiative properties of cirrus clouds for climate models, *J. Clim.*, 9, 2058–2082.
- Giangrande, S. E., S. Collis, J. Straka, A. Protat, C. Williams, S. Krueger, 2013: A Summary of Convective-Core Vertical Velocity Properties Using ARM UHF Wind Profilers in Oklahoma. *J. Appl. Meteor. Climatol.*, 52, 2278–2295.
- Giangrande, S. E., A. V. Ryzhkov, 2005: Calibration of Dual-Polarization Radar in the Presence of Partial Beam Blockage. *J. Atmos. Oceanic Technol.*, 22, 1156–1166.

- Gossard, E. E. (1994), Measurement of cloud droplet size spectra by Doppler radar. *J. Atmos. Oceanic Technol.*, 11, 712–726.
- Heymsfield, A. J., A. Bansemer, P. R. Field, S. L. Durden, J. L. Stith, J. E. Dye, W. Hall, C. A. Grainger (2002a), Observations and Parameterizations of Particle Size Distributions in Deep Tropical Cirrus and Stratiform Precipitating Clouds: Results from In Situ Observations in TRMM Field Campaigns. *J. Atmos. Sci.*, 59, 3457–3491.
- Heymsfield, A. J., S. Lewis, A. Bansemer, J. Iaquinta, L. M. Miloshevich, M. Kajikawa, C. Twohy, M. R. Poellot, (2002b): A General Approach for Deriving the Properties of Cirrus and Stratiform Ice Cloud Particles. *J. Atmos. Sci.*, 59, 3–29.
- Heymsfield, A. J., L. M. Miloshevich (2003): Parameterizations for the Cross-Sectional Area and Extinction of Cirrus and Stratiform Ice Cloud Particles. *J. Atmos. Sci.*, 60, 936–956.
- Heymsfield, A. J., Z. Wang, S.Y. Matrosov (2005), Improved Radar Ice Water Content Retrieval Algorithms Using Coincident Microphysical and Radar Measurements. *J. Appl. Meteor.*, 44, 1391–1412.
- Hong, G. (2007), Radar backscattering properties of nonspherical ice crystals at 94 GHz, *J. Geophys. Res.*, 112, D22203.
- Jensen, MP, W. Petersen, A. Del Genio, S. Giangrande, A. J. Heymsfield, G. M. Heymsfield, A. Hou, P. Kollias, B. Orr, S. Rutledge, M. Schwaller, E. Zipser (2010), Midlatitude Continental Convective Clouds Experiment (MC3E). DOE/SC-ARM/10-004, Dep. of Energy, Washington, D.C. [Available at <http://www.arm.gov/publications/programdocs/doe-sc-arm-10-004.pdf?id=66>]
- Kim, M. J. (2006), Single scattering parameters of randomly oriented snow particles at microwave frequencies, *J. Geophys. Res.*, 111, D14201.
- King, W. D., D. A. Parkin, R. J. Handsworth (1978), A Hot-Wire Liquid Water Device Having Fully Calculable Response Characteristics, *J. Appl. Meteor.*, 17, 1809–1813
- King, W. D., J. E. Dye, D. Baumgardner, J. W. Strapp, D. Huffman (1985), Icing Wind Tunnel Tests on the CSIRO Liquid Water Probe. *J. Atmos. Oceanic Technol.*, 2, 340–352
- Kollias, P., E. E. Clothiaux, M. A. Miller, B. A. Albrecht, G. L. Stephens, and T. P. Ackerman (2007), Millimeter-wavelength radars: New frontier in atmospheric cloud and precipitation research. *Bull. Amer. Meteor. Soc.*, 88, 1608–1624.

- Kollias, P., and Coauthors, 2014: Scanning ARM Cloud Radars. Part II: Data Quality Control and Processing. *J. Atmos. Oceanic Technol.*, 31, 583–598.
- Korolev, A. V., J. W. Strapp, G. A. Isaac, A. N. Nevzorov (1998), The Nevzorov Airborne Hot- Wire LWC–TWC Probe: Principle of Operation and Performance Characteristics, *J. Atmos. Oceanic Technol.*, 15, 1495–1510
- Liu, C. L., and A. J. Illingworth (1997), Error analysis of backscatter from discrete dipole approximation for different ice particle shapes, *Atmos. Res.*, 44, 231– 241.
- Liu, G. (2008), A Database of Microwave Single-Scattering Properties for Nonspherical Ice Particles, *Bull. Am. Meteorol. Soc.*, 89(10), 1,563–1,570.
- Lhermitte, R. (1990), Attenuation and scattering of millimeter wavelength radiation by clouds and precipitation. *J. Atmos. Oceanic Technol.*, 7, 464–479.
- Mace, G. G., A. J. Heymsfield, and M. R. Poellot (2002), On retrieving the microphysical properties of cirrus clouds using the moments of the millimeter-wavelength Doppler spectrum. *J. Geophys. Res.*, 107(D24), 4815.
- Mace, G. G., T. P. Ackerman, P. Minnis, and D. F. Young (1998), Cirrus layer microphysical properties derived from surface-based millimeter radar and infrared interferometer data, *J. Geophys. Res.*, 103, 23,207–23,216.
- Mace, G. G., Y. Zhang, S. Platnick, M. D. King, P. Minnis, P. Yang (2005): Evaluation of Cirrus Cloud Properties Derived from MODIS Data Using Cloud Properties Derived from Ground-Based Observations Collected at the ARM SGP Site. *J. Appl. Meteor.*, 44, 221–240
- Matrosov, S. Y. (1999), Retrieval of vertical profiles of ice cloud microphysics from radar and IR measurements using tuned regressions between reflectivity and cloud parameters. *J. Geophys. Res.*, 104, 16,741–16,753.
- Matrosov, S. Y (2005). "Attenuation-Based Estimates of Rainfall Rates Aloft with Vertically Pointing Ka-Band Radars." *J. Atmos. Oceanic Technol.*, 22 (1), 43-54
- Matrosov, S. Y., A. V. Korolev, and A. J. Heymsfield (2002), Profiling cloud ice mass and particle characteristic size from Doppler radar measurements. *J. Atmos. Oceanic Technol.*, 19, 1003–1018.
- McFarquhar, Greg M. (2004), A New Representation of Collision-Induced Breakup of Raindrops and Its Implications for the Shapes of Raindrop Size Distributions, *J. Atmos. Sci.*, 61, 777–794

- McFarquhar, Greg M., Michael S. Timlin, Robert M. Rauber, Brian F. Jewett, Joseph A. Grim, David P. Jorgensen (2007), Vertical Variability of Cloud Hydrometeors in the Stratiform Region of Mesoscale Convective Systems and Bow Echoes, *Mon. Wea. Rev.*, 135, 3405–3428
- Minnis, P. W. Heck, and D. F. Young (1993): Inference of cirrus cloud properties using satellite-observed visible and infrared radiances. Part II: Verification of theoretical cirrus radiative properties. *J. Atmos. Sci.*, 50, 1305–1322.
- Minnis, P., D. P. Garber, D. F. Young, R. F. Arduini, and Y. Takano (1998), Parameterization of reflectance and effective emittance for satellite remote sensing of cloud properties, *J. Atmos. Sci.*, 55, 3313–3339.
- Minnis, P., et al. (1995), Cloud Optical Property Retrieval (Subsystem 4.3). Clouds and the Earth's Radiant Energy System (CERES) Algorithm Theoretical Basis Document, volume III: Cloud Analyses and Radiance Inversions (Subsystem 4), NASA Tech. Rep. RP 1376, 135 – 176.
- Minnis, P., and W. L. Smith Jr.,(1998): Cloud and radiative fields derived from GOES-8 during SUCCESS and the ARM-UAV spring 1996 flight series. *Geophys. Res. Lett.*, 25, 1113–1116.
- Minnis, P., C. R. Yost, S. Sun-Mack, and Y. Chen (2008), Estimating the physical top altitude of optically thick ice clouds from thermal infrared satellite observations using CALIPSO data, *Geophys. Res. Lett.*, 35, L12801.
- Minnis, P., et al. (2011), CERES Edition-2 cloud property retrievals using TRMM VIRS and Terra and Aqua MODIS Data—Part I: Algorithms, *IEEE Trans. Geosci. Remote Sens.*, 49(11): 4374-4400
- Minnis P, Hong G, Ayers JK, Smith WL, Jr, Yost CR, Heymsfield AJ, Heymsfield GM, Hlavka DL, King MD, Korn E, McGill MJ, Selkirk HB, Thompson AM, Tian L, Yang P. (2012), Simulations of Infrared Radiances over a Deep Convective Cloud System Observed during TC4: Potential for Enhancing Nocturnal Ice Cloud Retrievals. *Remote Sensing.*; 4(10):3022-3054.
- Moran, K. P., B. E. Martner, M. J. Post, R. A. Kropfli, D. C. Welsh, and K. B. Widener (1998), An unattended cloud-profiling radar for use in climate research. *Bull. Amer. Meteor. Soc.*, 79, 443–455.
- Okamoto, H. (2002), Information content of the 95 GHz cloud radar signals: Theoretical assessment of effects of nonsphericity and error evaluations of the discrete dipole approximation, *J. Geophys. Res.*, 107(D22), 4628.

- Parol, F., J. C. Buriez, G. Brogniez, Y. Fouquart, 1991: Information Content of AVHRR Channels 4 and 5 with Respect to the Effective Radius of Cirrus Cloud Particles. *J. Appl. Meteor.*, 30, 973–984.
- Petersen. W and J. Michael (2012), The NASA-GPM and DOE-ARM Midlatitude Continental Convective Clouds Experiment (MC3E), *Earth obs.*, 24, 12-18
- Ryzhkov, A. V., S. E. Giangrande, V. M. Melnikov, T. J. Schuur (2005): Calibration Issues of Dual-Polarization Radar Measurements. *J. Atmos. Oceanic Technol.*, 22, 1138–1155.
- Sato, K., and H. Okamoto (2006), Characterization of Ze and LDR of nonspherical and inhomogeneous ice particles for 95-GHz cloud radar: Its implication to microphysical retrievals, *J. Geophys. Res.*, 111, D22213.
- Schneider, T. L., and G. L. Stephens (1995), Theoretical aspects of modeling backscattering by cirrus ice particles at millimeter wavelengths, *J. Atmos. Sci.*, 52, 4367–4385.
- Schumacher. C, R. A. Houze, I. Kraucunas, 2004: The Tropical Dynamical Response to Latent Heating Estimates Derived from the TRMM Precipitation Radar. *J. Atmos. Sci.*, 61, 1341–1358.
- Sherwood, S. C., J. - H. Chae, P. Minnis, and M. McGill (2004), Underestimation of deep convective cloud tops by thermal imagery, *Geophys. Res. Lett.*, 31, L11102.
- Smith, P.L., 1984: Equivalent Radar Reflectivity Factors for Snow and Ice Particles. *J. Climate Appl. Meteor.*, 23, 1258–1260.
- Smith, W. L., P. Minnis, H. Finney, R. Palikonda, and M. M. Khaiyer (2008), An evaluation of operational GOES-derived single-layer cloud top heights with ARSCL data over the ARM Southern Great Plains Site, *Geophys. Res. Lett.*, 35, L13820.
- Tao, W.-K., D. Wu, T. Matsui, C. Peters-Lidard, S. Lang, A. Hou, M. Rienecker, W. Peterson, and M. Jensen (2013), Precipitation intensity and variation during MC3E: A numerical modeling study, *J. Geophys. Res. Atmos.*, 118, 7199–7218
- Tao, W.-K., J. Simpson, S. Lang, M. McCumber, R. Adler and R. Penc, 1990: An algorithm to estimate the heating budget from vertical hydrometeor profiles. *J. Appl. Meteor.*, 29, 1232-1244.

- Turner, DD and KL Gaustad. (2004), "Improved PWV and LWP retrievals from the microwave radiometer for ARM." In Proceedings of the Fourteenth Atmospheric Radiation Measurement (ARM) Science Team Meeting, U.S. Department of Energy. Available URL: <http://www.arm.gov/publications/proceedings/conf14/author.stm>
- Tridon, F., A. Battaglia, P. Kollias, E. Luke and C. R. Williams, 2013: Signal postprocessing and reflectivity calibration of the Atmospheric Radiation Measurement 915-MHz wind profilers. *J. Atmos. Oceanic Technol.*, 30, 1038–1054.
- Wang, Z., and K. Sassen (2002), Cirrus cloud microphysical property retrieval using lidar and radar measurements: I. Algorithm description and comparison with in situ data, *J. Appl. Meteorol.*, 41, 218–229.
- Wang, Z., G. M. Heymsfield, L. Li, and A. J. Heymsfield (2005), Retrieving optically thick ice cloud microphysical properties by using airborne dual-wavelength radar measurements, *J. Geophys. Res.*, 110, D19201.
- Wielicki, B.A. et al. (1998), Clouds and the Earth's Radiant Energy System (CERES): Algorithm overview, *IEEE Trans. Geosci. Remote Sens.*, 36, 1127-1141.
- Widener, K., N. Bharadwaj, K. Johnson, Ka-Band ARM Zenith Radar (KAZR) (2012), DOE/SC-ARM/TR-106, Dep. of Energy, Washington, D.C. [Available at http://www.arm.gov/publications/tech_reports/handbooks/kazr_handbook.pdf]
- Wyser, K., and P. Yang (1998), Average ice crystal size and bulk shortwave single - scattering properties of cirrus clouds, *Atmos. Res.*, 49, 315–335.
- Yang, P., B. A. Baum, A. J. Heymsfield, Y. X. Hu, H.L. Huang, S.C. Tsay, and S. Ackerman (2003), Single scattering properties of droxtals, *J. Quant. Spectrosc. Radiat. Transfer*, 79-80, 1159-1169.
- Yost, C. R., P. Minnis, J. K. Ayers, D. A. Spangenberg, A. J. Heymsfield, A. Bansemmer, M. J. McGill, and D. L. Hlavka (2010), Comparison of GOES-retrieved and in situ measurements of deep convective anvil cloud microphysical properties during the Tropical Composition, Cloud and Climate Coupling Experiment (TC4), *J. Geophys. Res.*, 115, D00J06
- Zhao, C., S. Xie, S. A. Klein, A. Protat, M. D. Shupe, S. A. McFarlane, J.M. Comstock, J. Delanoë, M. Deng, M. Dunn, R. J. Hogan, D. Huang, M. P. Jensen, G. G. Mace, P. McCoy, E. J. OConnor, D. D. Turner and Z. Wang (2012), Toward understanding of differences in current cloud retrievals of ARM ground-based measurements, *J. Geophys. Res.*, 117, D10206.

Zhang, J., et al (2011), National Mosaic and Multi-Sensor QPE (NMQ) System: Description, Results and Future Plans. Bull.Amer.Meteor.Soc., 92(10), 1321-1338